EARTH SCIENCES

Continental igneous rock composition: A major control of past global chemical weathering

Clément P. Bataille,[1]* Amy Willis,[2] Xiao Yang,[1] Xiao-Ming Liu[1]*

The composition of igneous rocks in the continental crust has changed throughout Earth's history. However, the impact of these compositional variations on chemical weathering, and by extension on seawater and atmosphere evolution, is largely unknown. We use the strontium isotope ratio in seawater [$(^{87}Sr/^{86}Sr)_{seawater}$] as a proxy for chemical weathering, and we test the sensitivity of $(^{87}Sr/^{86}Sr)_{seawater}$ variations to the strontium isotopic composition ($^{87}Sr/^{86}Sr$) in igneous rocks generated through time. We demonstrate that the $^{87}Sr/^{86}Sr$ ratio in igneous rocks is correlated to the epsilon hafnium (εHf) of their hosted zircon grains, and we use the detrital zircon record to reconstruct the evolution of the $^{87}Sr/^{86}Sr$ ratio in zircon-bearing igneous rocks. The reconstructed $^{87}Sr/^{86}Sr$ variations in igneous rocks are strongly correlated with the $(^{87}Sr/^{86}Sr)_{seawater}$ variations over the last 1000 million years, suggesting a direct control of the isotopic composition of silicic magmatism on $(^{87}Sr/^{86}Sr)_{seawater}$ variations. The correlation decreases during several time periods, likely reflecting changes in the chemical weathering rate associated with paleogeographic, climatic, or tectonic events. We argue that for most of the last 1000 million years, the $(^{87}Sr/^{86}Sr)_{seawater}$ variations are responding to changes in the isotopic composition of silicic magmatism rather than to changes in the global chemical weathering rate. We conclude that the $(^{87}Sr/^{86}Sr)_{seawater}$ variations are of limited utility to reconstruct changes in the global chemical weathering rate in deep times.

INTRODUCTION

The chemical weathering of silicates transfers elements from the continental crust to seawater and exerts a direct control on several biogeochemical cycles. For instance, chemical weathering of silicates transfers calcium (Ca) and magnesium (Mg) to seawater and regulates atmospheric carbon dioxide levels and temperature at the surface by controlling the rate of marine carbonate precipitation (*1*). Despite decades of research, the mechanisms controlling chemical weathering throughout Earth's history remain highly debated (*2*). The flux of elements from continental weathering to seawater is thought to be primarily controlled by the rate of chemical weathering. This rate depends mostly on runoff, temperature, and erosion and is thus modulated through time by changes in topography (*3*, *4*), paleogeography (*5*), climate (*5*–*7*), and biological evolution (*8*, *9*). The type of rock being weathered is also a critical parameter in understanding chemical weathering because minerals have distinct chemical composition and dissolution kinetics (*10*). However, the chemical composition of rocks subject to weathering is usually not accounted for when reconstructing the long-term changes in global chemical weathering.

The interpretation of the strontium isotope ratio in seawater [$(^{87}Sr/^{86}Sr)_{seawater}$] is a good illustration of this issue. The $(^{87}Sr/^{86}Sr)_{seawater}$ variations are commonly used to estimate changes in global chemical weathering rates throughout Earth's history (*11*). The $(^{87}Sr/^{86}Sr)_{seawater}$ curve displays an overall exponential increase controlled by the progressive differentiation of the Earth's crust and the associated increase in the rubidium-to-strontium ratio (Rb/Sr) (*11*, *12*). This trend is superimposed by second-order fluctuations at the scale of tens of million years, which are interpreted as reflecting changes in the relative Sr flux from isotopically distinct sources (*11*–*15*). This interpretation assumes that the $^{87}Sr/^{86}Sr$ ratios of the radiogenic and unradiogenic Sr sources change too slowly or are not large enough to control the $(^{87}Sr/^{86}Sr)_{seawater}$ variations (*11*). For instance, the steep rise in $(^{87}Sr/^{86}Sr)_{seawater}$ ratio in the last 40 million years (My) has been explained by several competing "flux"-based hypotheses, including (i) an enhanced radiogenic Sr flux from radiogenic continental surfaces associated with uplift (*3*, *16*) or glacial processes (*7*, *17*, *18*) and (ii) a decreased unradiogenic Sr flux from the oceanic crust associated with slower seafloor spreading rate (*19*) or cooler ocean temperature (*20*). Rapid changes in the composition of the $^{87}Sr/^{86}Sr$ ratio of continental surfaces have been invoked to explain some more specific features in the $(^{87}Sr/^{86}Sr)_{seawater}$ curve. For instance, the emplacement of large igneous provinces (LIPs) or the uplift of ophiolites can rapidly decrease the average $^{87}Sr/^{86}Sr$ ratio from continental weathering (*21*–*23*), whereas the weathering of Sr-rich radiogenic metalimestones could raise the $^{87}Sr/^{86}Sr$ of rivers (*24*, *25*). In contrast, little attention has been given to the potential variations in the average $^{87}Sr/^{86}Sr$ ratio in igneous rocks generated at plate margins. Plate margin magmatism is the dominant contributor to new continental crust (*26*, *27*) and serves as parent rock to a large portion of the siliciclastic sediments of Earth's surface (*28*). The $^{87}Sr/^{86}Sr$ ratios in silicic rocks generated in this tectonic setting are more variable than those in basalts (*29*, *30*), and the impact of these compositional variations on the $(^{87}Sr/^{86}Sr)_{seawater}$ variations has not been explored.

Erosion and burial remove rocks from the surface through time, which complicates the reconstruction of the compositional evolution of igneous rocks (*31*). Fortunately, eroded components of rocks, such as zircon, are preserved in the siliciclastic sedimentary record. Zircon grains can survive multiple sedimentary cycles, because of their resistance to physiochemical alteration (*32*), and contain a wealth of geochemical information on their hosting igneous rock (*32*). Uranium-lead dating (U-Pb date) provides precise crystallization age of the zircon grains, whereas epsilon hafnium (εHf) records the degree to which a melt incorporates juvenile mantle versus reworked preexisting crust sources (*32*). Large compilations of integrated U-Pb date and εHf from detrital zircon have been used to reconstruct the evolution of the continental crust throughout Earth's history (*33*–*36*). However, generation and preservation biases in the detrital zircon

[1]Department of Geological Sciences, University of North Carolina at Chapel Hill, Chapel Hill, NC 27599, USA. [2]Department of Statistical Science, Cornell University, Ithaca, NY 14853, USA.
*Corresponding author. Email: cbataill@email.unc.edu (C.P.B.); xiaomliu@unc.edu (X.-M.L.)

record complicate the interpretation of the secular εHf variations through time (*35*). Mafic rocks (high-temperature, low-silica dry magmas) have low-zircon fertility in comparison with felsic rocks (low-temperature, high-silica hydrous magmas) (*28*, *37*, *38*). Zircon grains generated in intraplate volcanism, late accretionary, and collisional tectonic settings are preferentially preserved in sediments relative to those generated in extensional tectonic setting (*39*–*43*). Ultimately, the detrital zircon record is likely biased toward silicic igneous rocks generated in intraplate volcanism or convergent margins, although the debate on this question is far from being resolved (*28*, *33*, *35*, *37*, *38*, *41*, *42*, *44*). Acknowledging the biases outlined above, we used the detrital zircon record to reconstruct the initial $^{87}Sr/^{86}Sr$ ratio of zircon-bearing igneous rocks [$(^{87}Sr/^{86}Sr)_{i\text{-}zig}$] over the last 1000 My. We discuss the strengths and limitations of this record, and we reinterpret the $(^{87}Sr/^{86}Sr)_{seawater}$ variations over the last 1000 My by accounting for the changes in isotopic composition of igneous rocks generated through time.

RESULTS

Here, we present a method to reconstruct the $(^{87}Sr/^{86}Sr)_{i\text{-}zig}$ variations for the last 1000 My. We compiled a first database gathering integrated U-Pb date and Hf isotopes on detrital zircon grains from globally distributed siliciclastic sediments (database S1). Detailed metadata are used to filter the data to minimize the issues associated with the use of combined U-Pb and Hf isotopes on detrital zircon grains (see Materials and Methods and the Supplementary Materials). The screened database gathers integrated U-Pb date and Hf isotopes from 24,715 zircon grains from 535 individual Mesozoic and Cenozoic sediments (Fig. 1). A debiasing method based on bootstrap resampling was applied to the compiled data set to correct for geographic and sampling biases in the detrital zircon record (see Materials and Methods and the Supplementary Materials). To account for the uncertainty in εHf and U-Pb date of individual zircon grains, we performed the resampling with introduction of Gaussian noise scaled to the εHf value and U-Pb date of the grains (see Materials and Methods and the Supplementary Materials). Using the resampled data set, we applied a smoothing procedure to obtain an approximately unbiased estimate of the εHf in detrital zircon grains through time (Fig. 1). The sensitivity of the smoothed trend to different weighing schemes, uncertainty levels, and resampling strategies was also tested to verify the robustness of our results (see Materials and Methods and the Supplementary Materials).

We compiled a second database combining whole-rock strontium isotope ratio ($^{87}Sr/^{86}Sr$) data with integrated U-Pb date and Hf isotopes from magmatic zircon for Phanerozoic igneous rocks (database S2). The epsilon strontium (εSr) of the whole-rock samples and the εHf of the associated zircon grains were calculated. We screened the database to minimize uncertainty in the εHf and εSr calculations (see Materials and Methods and the Supplementary Materials). The screened data set gathers 351 individual igneous rock samples with combined εSr whole-rock and associated average integrated U-Pb date and Hf isotopes from their hosted magmatic zircon grains. The εHf of zircon grains correlates with the εSr of their hosting igneous rock, reflecting the coupling between the Sr and Hf isotope systems in magmatic processes (Fig. 2). However, Hf and Sr can be decoupled, with Hf always being incompatible and Sr becoming compatible once plagioclase crystallization begins (*45*). This decoupling, as well as the broad range of Sr and Hf content in the parent magma, explains the scatter in the correlation between εHf and εSr. It should be noted that the screening procedure did not significantly change the correlation equation between whole-rock εSr and the average εHf of hosted magmatic zircon grains. We used the relationship between the εHf of zircon grains and the εSr of their hosting igneous rocks to estimate the secular variations in the $(^{87}Sr/^{86}Sr)_{i\text{-}zig}$ for the last 1000 My (Fig. 2). Secular changes in the $(^{87}Sr/^{86}Sr)_{i\text{-}zig}$ ratio reflect the changing proportion of juvenile and reworked materials generated in orogenies through time and vary with the supercontinent cycle (*46*).

We compared the smoothed $(^{87}Sr/^{86}Sr)_{i\text{-}zig}$ ratio curve with the variations of the $(^{87}Sr/^{86}Sr)_{seawater}$ ratio through time (Fig. 3). To facilitate the time series analysis, we built upon previous work (*12*) to normalize the $(^{87}Sr/^{86}Sr)_{seawater}$ variations [$N(^{87}Sr/^{86}Sr)_{seawater}$] (see Materials and Methods and the Supplementary Materials). To normalize this curve, we removed from the $(^{87}Sr/^{86}Sr)_{seawater}$ curve the signal associated with the radiogenic decay of the crust (Fig. 3A) (*47*). The $N(^{87}Sr/^{86}Sr)_{seawater}$ curve correlates with the $(^{87}Sr/^{86}Sr)_{i\text{-}zig}$ curve over

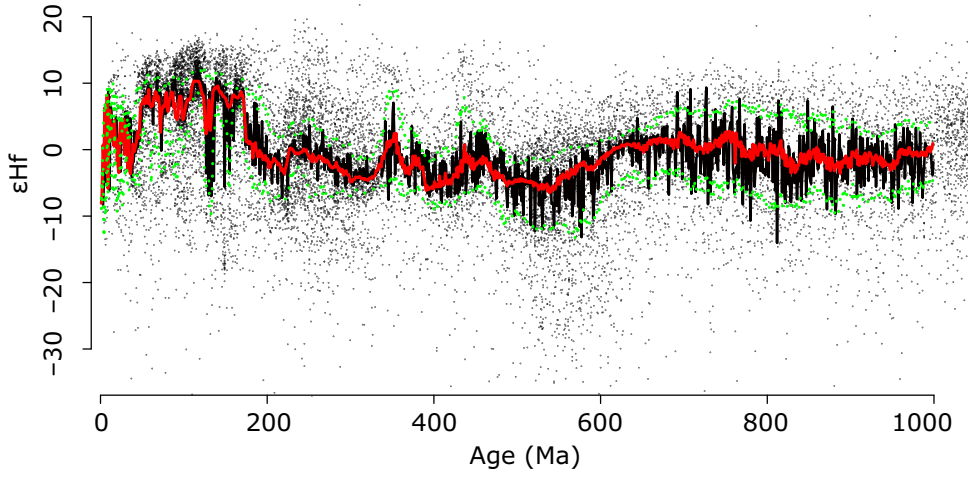

Fig. 1. Plot of εHf of detrital zircon grains versus U-Pb date. Black dots represent the nonresampled εHf data from a screened subset of database S1. Moving median and quartiles at 1-My increments for the resampled database S1 (red line and green lines) and for the nonresampled database S1 (black line). The resampled data set includes both the debiasing resampling and the uncertainty propagation resampling (see Materials and Methods and the Supplementary Materials). The uncertainty propagation resampling uses U-Pb date (±2%) and εHf (±0.62).

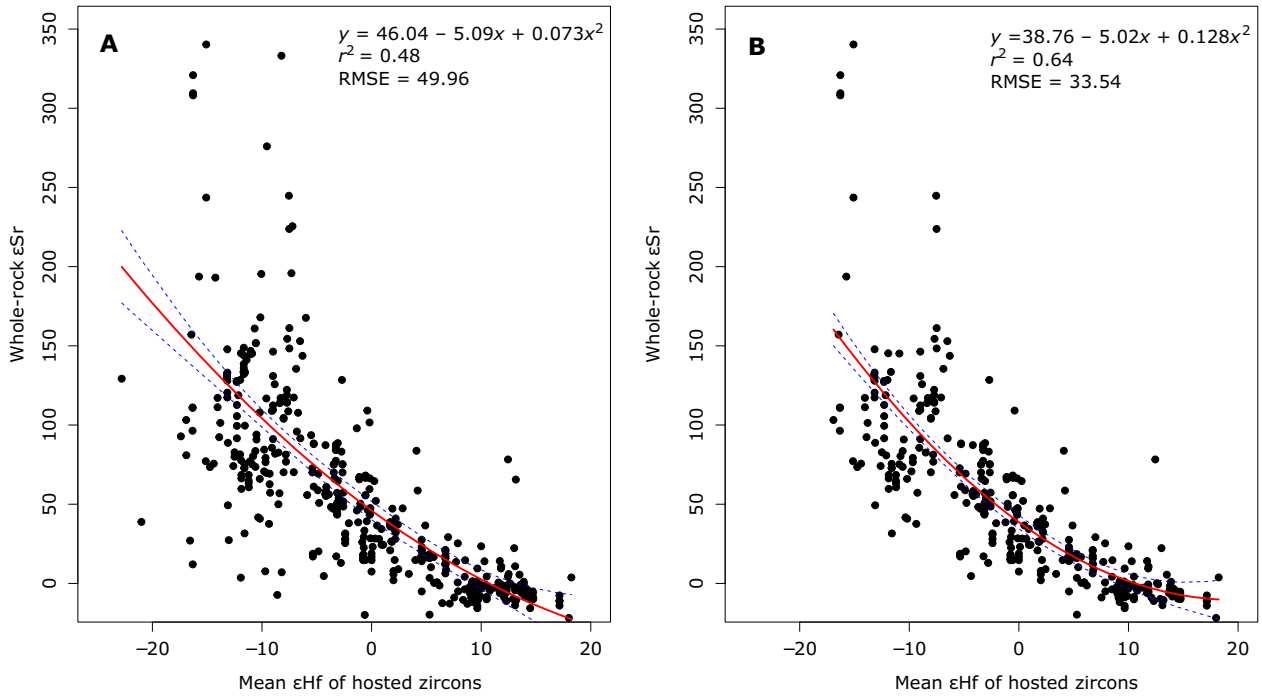

Fig. 2. Plot of εHf values of inherited zircon grains versus whole-rock εSr values for Phanerozoic igneous rocks. (**A**) Nonscreened database S2. (**B**) Screened database S2. Screening procedure removed rock with crystallization age older than 300 Ma and with $^{87}Rb/^{86}Sr$ superior to 40. Regression models fitted to the data (red lines) with 95% confidence interval (blue lines). RMSE, root mean square error.

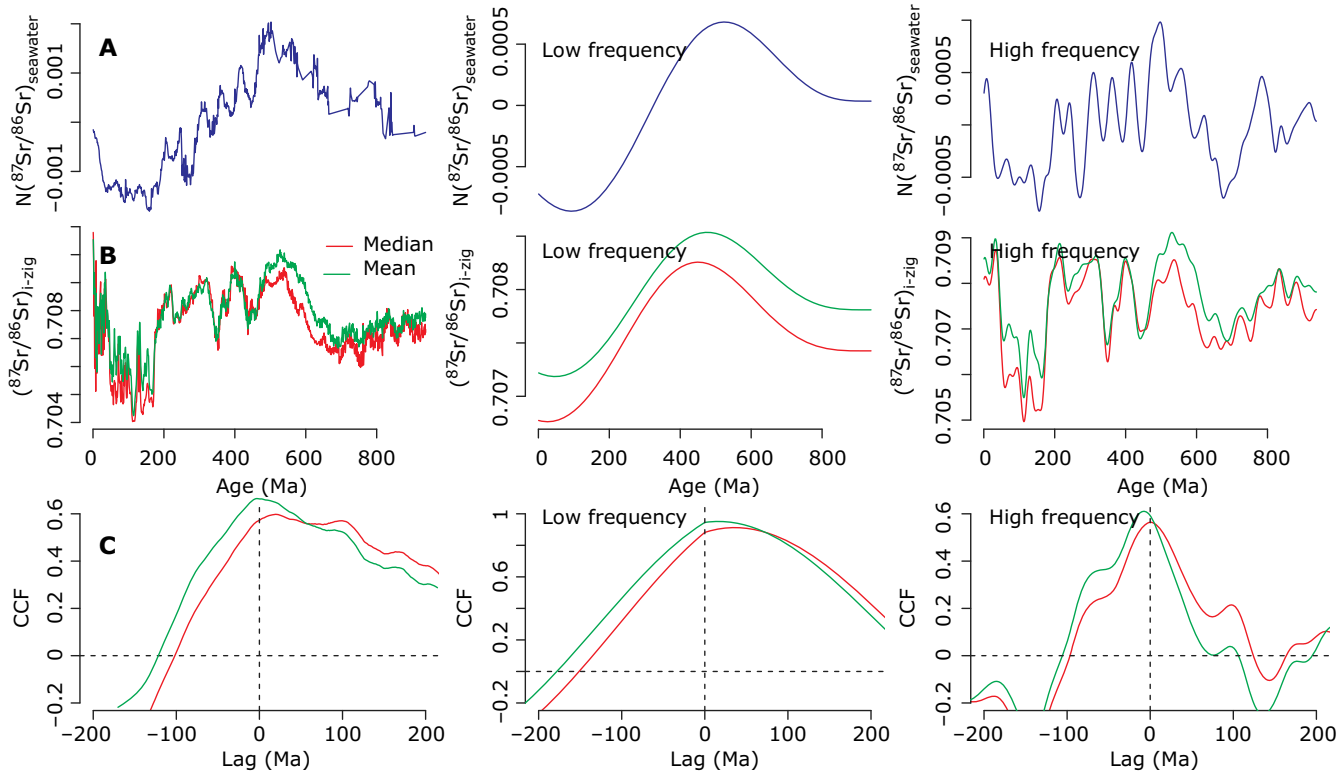

Fig. 3. Time series analysis between $N(^{87}Sr/^{86}Sr)_{seawater}$ (blue) and the median (red) and mean (green) $(^{87}Sr/^{86}Sr)_{i\text{-}zig}$, both decomposed to their slow-varying trend and fast-varying residues. $N(^{87}Sr/^{86}Sr)_{seawater}$ ratio (**A**) and $(^{87}Sr/^{86}Sr)_{i\text{-}zig}$ ratio (**B**) as in Fig. 1. (**C**) CCF. The first column corresponds to the original data at a 1-My interpolated sampling interval, the second column corresponds to the signal filtered for 700-My or longer periodicity, and the third column corresponds to the residual filtered between 30- and 700-My periodicity. The range of lags tested was set at ±200 My to include slowly exhumed plutonic rocks. A negative lag corresponds to the $N(^{87}Sr/^{86}Sr)_{seawater}$ ratio lagging the $(^{87}Sr/^{86}Sr)_{i\text{-}zig}$ ratio.

the last 1000 My (Fig. 3). The highest correlation [cross-correlation function (CCF) > 0.65] occurs when the time series are centered on each other (lag = 0 ± 20 My), with the correlation decreasing rapidly for time lags larger than 20 My (Fig. 3C). To test the strength of the correlation at different periodicity, we decomposed both $N(^{87}Sr/^{86}Sr)_{seawater}$ and $(^{87}Sr/^{86}Sr)_{i\text{-}zig}$ curves into a slow-varying trend component and a fast-varying component by applying two respective fourth-order Butterworth filters (see Materials and Methods and the Supplementary Materials). The signals show a high correlation (CCF ≈ 0.6) for periodicities above 30 My. The correlation decreases for periodicity shorter than 30 My likely because of the uncertainty in U-Pb date and εHf value, which make the $(^{87}Sr/^{86}Sr)_{i\text{-}zig}$ ratio increasingly noisy. We tested the sensitivity of the correlation between these time series to our weighing scheme and normalization procedure and found the correlation between these curves to be robust and independent of our data analysis choices.

DISCUSSION

We interpret the correlation between the $N(^{87}Sr/^{86}Sr)_{seawater}$ and the $(^{87}Sr/^{86}Sr)_{i\text{-}zig}$ variations over the last 1000 My as reflecting a direct control of the isotopic composition of silicic igneous rocks on the $(^{87}Sr/^{86}Sr)_{seawater}$ variations. We suggest that when the global isotopic composition of silicic igneous rocks increases, the rapid cycling and subsequent weathering of these rocks lead to an increase in the $(^{87}Sr/^{86}Sr)_{seawater}$ ratio within a relatively short time period (<20 My). The $(^{87}Sr/^{86}Sr)_{i\text{-}zig}$ variations probably reflect the changes in the relative proportion of evolved to less evolved magmas generated in orogenies and subduction zones during different stages of the supercontinent cycle (*46*, *48*). Here, we reinterpret the $(^{87}Sr/^{86}Sr)_{seawater}$ variations over the last 1000 My by accounting for this compositional variable. We also propose alternative hypotheses that could explain the correlation between these time series.

The $N(^{87}Sr/^{86}Sr)_{seawater}$ and the $(^{87}Sr/^{86}Sr)_{i\text{-}zig}$ ratios correlate strongly over different periodicities (Fig. 3C). Igneous rocks forming during collisional magmatism, accretionary orogenies in advancing phase (for example, Andean orogeny), and mature island arcs are characterized by a high reworking of older crust and have high $(^{87}Sr/^{86}Sr)_{i\text{-}zig}$ values (*46*, *48*). In contrast, igneous rocks forming in island arcs, extensional arcs, or accretionary orogenies in retreating phase (rollback) are less evolved and have low $(^{87}Sr/^{86}Sr)_{i\text{-}zig}$ values (*46*, *48*). We thus suggest that the overall high $N(^{87}Sr/^{86}Sr)_{seawater}$ ratio between 600 and 300 Ma (million years ago) reflects the continued assembly of the Gondwana-Pannotia and Pangea supercontinents (*46*). During that period, collisional orogenies are frequent and subduction occurs dominantly in advancing phase, with the opening of several ocean basins forming igneous rocks with high $(^{87}Sr/^{86}Sr)_{i\text{-}zig}$ ratios (*46*). The lower $N(^{87}Sr/^{86}Sr)_{seawater}$ ratios before 700 Ma and between 250 and 100 Ma might reflect the increased proportion of less evolved island and extensional arcs as well as the long-term closing of ocean basins during the assembly of the Gondwana-Pannotia and Amasia supercontinents, respectively. During those periods, subduction zones are more frequently in retreating phase forming immature arcs with lower $(^{87}Sr/^{86}Sr)_{i\text{-}zig}$ ratios (Fig. 3A) (*46*). Interpreting the $(^{87}Sr/^{86}Sr)_{i\text{-}zig}$ fluctuations on a shorter time scale is more ambiguous because of the bias in the detrital zircon record, the overlapping of breakup and assembly phases, and the difference in the supercontinent assembly mode between Pangea and Gondwana (that is, introversion versus extroversion) (*46*). However, we argue that the $(^{87}Sr/^{86}Sr)_{i\text{-}zig}$ fluctuations track the global evolution of the isotopic composition of silicic magmatism occurring at plate boundaries through time and that these isotopic fluctuations are rapidly transmitted to seawater through erosion and weathering.

Two prerequisites for this interpretative framework to be valid are as follows: (i) the amplitude of $(^{87}Sr/^{86}Sr)_{i\text{-}zig}$ variations and the magnitude of the Sr flux from young zircon-bearing igneous rocks have to be significant enough to affect the marine Sr isotope budget, and (ii) young zircon-bearing igneous rocks have to be cycled (that is, exhumed and weathered) rapidly on the surface (<20 My) for the time series to be synchronized (Fig. 3C). The reconstructed $(^{87}Sr/^{86}Sr)_{i\text{-}zig}$ ratio ranges from ~0.704 to ~0.710 for the last 1000 My (Fig. 4C). Given this range, the flux of Sr from zircon-bearing igneous rocks needs to contribute around half of the total Sr flux to control the totality of the $N(^{87}Sr/^{86}Sr)_{seawater}$ variations. Zircon-bearing igneous rocks represent only ~10% of the silicates exposed on Earth's surface at the present day (*49*). Young igneous rocks and associated volcaniclastic sediments

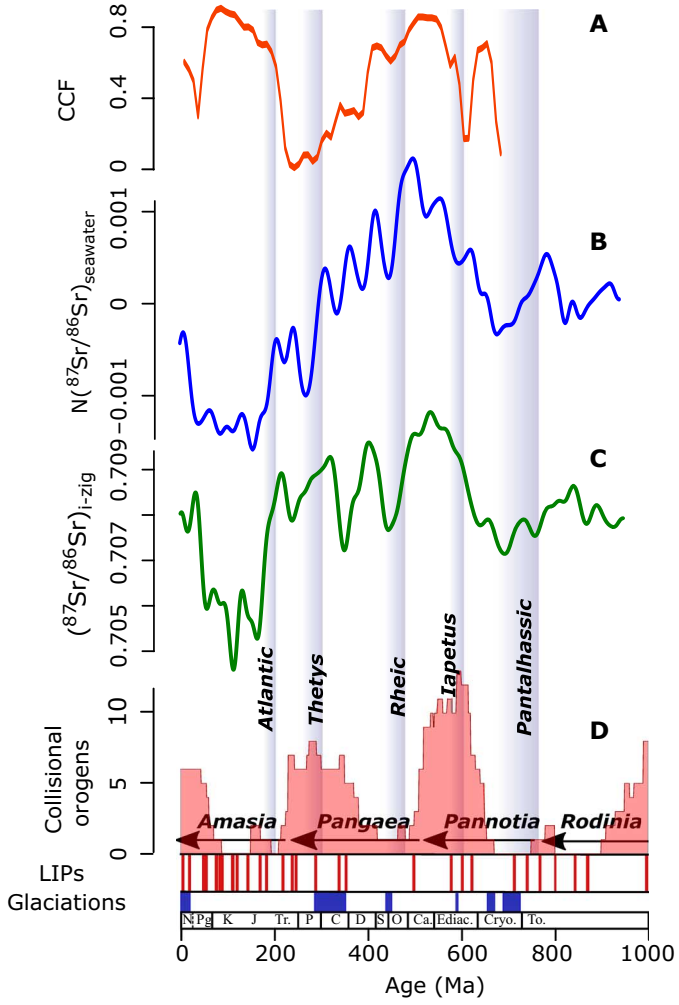

Fig. 4. Interpretation of the marine Sr budget. Maximum correlation coefficient through time (**A**) between the $N(^{87}Sr/^{86}Sr)_{seawater}$ ratio (**B**) and the $(^{87}Sr/^{86}Sr)_{i\text{-}zig}$ ratio (green) (**C**). Curves (B) and (C) are obtained by summing the slow-varying trend and fast-varying residues of the mean value obtained in Fig. 3 (A and B, respectively). The CCF is calculated for a 150-My time window moving in 10-My increments, with lags ranging between 0 and 20 My. (**D**) Frequency of collisional orogenies (*46*), major LIPs (*23*, *314*), and major glaciations. Shaded blue bars represent ocean opening stages.

are usually highly weatherable, exhumed rapidly, and uplifted which favors a very high solute flux from these rocks (*50*–*53*). At the present day, young igneous rocks (including basalts) contribute more than a third of the total Sr flux to seawater (*50*, *52*, *53*). Together, these observations suggest a large contribution of young igneous rocks to the Sr budget in seawater.

The strength of the correlation between the time series is not uniform through time (Fig. 4A). Periods of high correlation (CCF > 0.7) coincide with supercontinent dispersal and assembly stages (Fig. 4D) (*50*). This observation suggests that during periods when plate margins are dominated by subduction magmatism, the $(^{87}Sr/^{86}Sr)_{i\text{-}zig}$ variations, associated with changes in the relative proportion of evolved versus less evolved arcs, are the dominant factor of $N(^{87}Sr/^{86}Sr)_{seawater}$ variations. One issue with this interpretation is that the detrital zircon record, and hence $(^{87}Sr/^{86}Sr)_{i\text{-}zig}$ variations, does not record in equal proportion between evolved and less evolved magmatism because zircons are preferentially formed in silicic magmas (*37*, *41*). Hence, the sensitivity of the $(^{87}Sr/^{86}Sr)_{i\text{-}zig}$ variations to magmatism from less evolved arcs remains unknown. At the present day, less evolved arcs contribute significantly to the Sr budget in seawater and are likely to have been an important source of Sr to the ocean in the past (*52*). Owing to the large volume of magma generated during less evolved arc magmatism (*42*), zircon grains from this tectonic setting might still be the dominant control of the reconstructed $(^{87}Sr/^{86}Sr)_{i\text{-}zig}$ ratio during periods dominated by this style of magmatism. Another possibility to explain the strength of the correlation is that if the rates of mid-ocean ridge magmatism and subduction magmatism are at steady state (*54*, *55*), then the combined Sr flux from these sources should be relatively constant through time. As the $^{87}Sr/^{86}Sr$ ratio of basalts generated in mid-oceanic ridges and less evolved arcs varies little through time (*29*), the isotopic composition of the combined subduction and mid-oceanic ridge Sr fluxes should be mostly sensitive to the $^{87}Sr/^{86}Sr$ variations of silicic magmatism in more evolved arcs. In any cases, the strong correlation between $(^{87}Sr/^{86}Sr)_{i\text{-}zig}$ and $N(^{87}Sr/^{86}Sr)_{seawater}$ variations through most of the last 1000 My suggests a strong control of the isotopic composition of silicic arcs on the $(^{87}Sr/^{86}Sr)_{seawater}$ variations.

Periods with a low correlation coefficient (CCF < 0.5) between the time series could be explained by the following: (i) the incomplete geographic coverage, potential biases, and/or uncertainty in the detrital zircon database or (ii) the decoupling between εHf and εSr in magmatic processes (Fig. 2). However, we notice that intervals when the time series are not correlated coincide with specific paleogeographic, tectonic, or climatic events. We suggest that although the relative proportion of evolved versus less evolved arcs is the primary driver of $(^{87}Sr/^{86}Sr)_{seawater}$ variations, the remaining variance could be explained by changes in the relative Sr fluxes from isotopically distinct sources associated with paleogeographic, tectonic, or climatic events. Our reconstructed $(^{87}Sr/^{86}Sr)_{i\text{-}zig}$ variations do not account for the radiogenic Sr flux from radiogenic recycled silicates, the unradiogenic Sr flux from mid-oceanic ridges, or the Sr flux from recycled carbonates. Although the relative Sr fluxes and isotopic composition from these sources might be relatively constant over long time periods, a shift in the relative flux from one of these isotopically distinct sources will alter the correlation between $(^{87}Sr/^{86}Sr)_{i\text{-}zig}$ and $(^{87}Sr/^{86}Sr)_{seawater}$ variations. The correlation coefficient decreases during the Cryogenian, the Early Ediacaran, and the Neogene periods. During these periods, the $(^{87}Sr/^{86}Sr)_{i\text{-}zig}$ values decrease, whereas the $(^{87}Sr/^{86}Sr)_{seawater}$ values increase, indicating a "missing" radiogenic component to the Sr isotope budget in seawater (Fig. 4C). These periods coincide with time when the rate of collisional orogenies was high and/or when the climate was in an icehouse period (Fig. 4). During periods of collisional orogenies or during icehouse periods, increased erosion might increase the radiogenic Sr flux relative to the unradiogenic Sr flux (Fig. 4) (*3*, *18*). The correlation between the time series also decreases during the amalgamation of the Pangea supercontinent. However, during this period, the $(^{87}Sr/^{86}Sr)_{i\text{-}zig}$ values increase, whereas the $(^{87}Sr/^{86}Sr)_{seawater}$ values decrease (Fig. 4C). Global runoff has been relatively constant over long time scale, and only a few paleogeographic configurations have led to significant runoff changes in the last 1000 My (*5*, *56*). During Pangea amalgamation, increased continental interior aridity led to a twofold decrease of the global runoff relative to other time periods, which would have largely decreased the radiogenic Sr flux from cratonic areas (*5*). This progressive decrease in Sr flux from radiogenic continental areas combined with the increase in mid-oceanic ridge magmatism associated with the Tethys opening might explain the lower $(^{87}Sr/^{86}Sr)_{seawater}$ values during the Permian period (*57*). Changes in the isotopic signature of the Sr flux exported from continents are associated with the uplift of metamorphic rocks, ophiolites, and LIPs (*22*) can also play a significant role in the Sr isotope budget (*56*). The rapid weathering of these isotopically distinct rocks in favorable paleogeographic or tectonic configuration likely contributes to some of the $(^{87}Sr/^{86}Sr)_{seawater}$ variations over the last 1000 My (Fig. 4).

An alternative and/or complementary interpretation to explain the correlation between the $(^{87}Sr/^{86}Sr)_{i\text{-}zig}$ and $(^{87}Sr/^{86}Sr)_{seawater}$ ratios is that the generation and preservation biases of the detrital zircon record correlate to changes in Sr flux from radiogenic and unradiogenic sources of Sr. The $(^{87}Sr/^{86}Sr)_{seawater}$ variations are thought to be highly dependent on the rate of collisional orogenies because of the potential large increase in the Sr flux from uplifted recycled silicates with radiogenic isotopic signatures (*3*, *16*, *25*). During periods when both collisional orogenies and subduction magmatism occur, the global detrital zircon record will display a high global zircon count associated with generation and/or preservation biases (*42*, *43*). The detrital zircon record will be biased toward magmatism occurring during collisional orogenies and/or arc magmatism preserved in this convergent tectonic setting (*43*). The zircon grains generated in this tectonic setting might have a more radiogenic isotopic signature that will bias the $(^{87}Sr/^{86}Sr)_{i\text{-}zig}$ variations toward higher values. These high $(^{87}Sr/^{86}Sr)_{i\text{-}zig}$ values could coincide with an increase in the weathering rate of uplifted radiogenic recycled silicates (Fig. 4). Conversely, during periods with no collisional orogenies, the global detrital zircon record will display a low global zircon count associated with generation and/or preservation biases (*42*, *43*). The reconstructed $(^{87}Sr/^{86}Sr)_{i\text{-}zig}$ ratio might be lower during these periods, reflecting the higher contribution of zircon grains with low $(^{87}Sr/^{86}Sr)_{i\text{-}zig}$ ratio (*46*). These low $(^{87}Sr/^{86}Sr)_{i\text{-}zig}$ values could coincide with increased Sr flux from unradiogenic basalts at island arcs or mid-oceanic ridges as observed for the Mesozoic (Fig. 4). However, this framework requires that magmatism associated or preserved during collisional orogeny has a distinct isotopic signature relative to other magmatism preserved in the detrital zircon record (*43*, *46*, *48*, *58*). This might be true for some supercontinents and some collisional orogenies, but it also depends on the mode of supercontinent assembly and the type of arcs preserved during collision (*43*, *46*, *58*).

In summary, we present a new method to reconstruct the evolution of the strontium isotopic composition of silicic igneous rocks through time. We argued that the $(^{87}Sr/^{86}Sr)_{i\text{-}zig}$ variations are the dominant control of $(^{87}Sr/^{86}Sr)_{seawater}$ evolution over the last 1000 My. Instead of

interpreting $(^{87}Sr/^{86}Sr)_{seawater}$ variations as reflecting changes in the chemical weathering rate of radiogenic continental surfaces, we suggest that they primarily track the relative proportion of evolved versus less evolved magmas in the continental crust. These changes in the global isotopic composition of silicic magmas are likely controlled by the different types of orogeny and the variations in subduction phases occurring with distinct supercontinent cycle stages. The remaining $(^{87}Sr/^{86}Sr)_{seawater}$ variations are probably explained by changes in the relative Sr flux from isotopically distinct sources associated with specific paleogeographic configurations, mountain-building events, emplacement of LIPs, or climate variations. We conclude that the $(^{87}Sr/^{86}Sr)_{seawater}$ variations are of limited utility to reconstruct the long-term chemical weathering rate.

MATERIALS AND METHODS

Database compilation and screening procedures

Database S1.

We assembled a geochemical database with integrated U-Pb date and Hf isotopes from a total of 183 individual studies (*34*, *59*–*241*), including some from preexisting compilations (database S1) (*35*, *36*, *46*, *90*, *242*). We added a large number of Mesozoic and Cenozoic samples from regions that were underrepresented in previous databases, such as the North American Cordillera, the South American Cordillera, Antarctica, the Middle East, Turkey, and Australia. Each sample was paired with a geospatial location. Additional data from rivers in Europe and western Africa would be required to fill geographic gaps. When location was not given, we used Google Earth and metadata from the study to estimate the approximate latitude and longitude of the samples. Other metadata compiled include the lithostratigraphic description of the sediment, age of deposition, instrument used for analysis, and range of Th/U ratio and cathodoluminescence description of the samples. For each zircon grain present in the databases, we also calculated εHf using Eq. (1). The result is a data set including up to 37 defined variables for each of the compiled samples from varied geographic locations. These detailed metadata were used to filter the database and to minimize the issues associated with the use of combined U-Pb and Hf isotope on detrital zircon grains (*36*, *243*). To minimize crystallization age and analytical uncertainty on εHf calculation, we only selected the following: (i) zircon grains analyzed using in situ analysis, (ii) zircon grains with high U-Pb date concordance (<10%), and (iii) zircon grains with low analytical uncertainty and isobaric interferences $^{176}Yb/^{177}Hf < 0.2$ or $^{176}Lu/^{177}Hf < 0.005$. To minimize the possible impact of mixed sampling of complex zircon grains, we screened zircon grains that were reportedly affected by metamorphism using Th/U ratio (Th/U < 0.05) and/or visual occurrence of metamorphic rims from cathodoluminescence. The resulting database contains 54,406 zircon grains with integrated U-Pb date and Hf isotopes from 1263 individual siliciclastic sediments.

Database S2.

We compiled a second database combining whole-rock $^{87}Sr/^{86}Sr$ ratio data and average integrated U-Pb date and Hf isotopes from hosted magmatic zircon grains from 60 individual studies (database S2) (*244*–*304*). For each whole rock, we calculated εSr using Eq. (1). We compiled igneous rocks data only from the Phanerozoic to minimize the uncertainty in the εSr calculations. The data set contains 441 analyses of $^{87}Sr/^{86}Sr$ data from whole igneous rocks coupled with the average U-Pb date and Hf isotopes from their hosted magmatic zircon grains. We used this database to relate the εHf of zircon grains with the εSr of their hosting igneous rock (Fig. 2). We first attempted to minimize uncertainty in εSr calculations by filtering data with the highest analytical or calculation uncertainty. At equal age, whole rock with very high Rb/Sr ratio will have a higher uncertainty in their calculated εSr. Similarly, at equal Rb/Sr ratio, older rocks will have a higher uncertainty in the εSr calculation. We tested several thresholds of Rb/Sr and age uncertainty and found that keeping whole-rock data younger than 300 Ma and with $^{87}Rb/^{86}Sr$ inferior to 40 led to the best improvement in correlation coefficient and root mean square error. This screening effectively removes 90 εSr from the data set or ~20% of the data.

Epsilon value calculation.

The formula used to calculate the epsilon value is given below for the Hf isotope system, but the formula is also valid for the strontium isotope system

$$\varepsilon Hf(t) = \left(\frac{\left(\frac{^{176}Hf}{^{177}Hf}\right)_{sample}(t)}{\left(\frac{^{176}Hf}{^{177}Hf}\right)_{CHUR}(t)} - 1 \right) \times 10,000 \quad (1)$$

where $(^{176}Hf/^{177}Hf)_{sample}$ and $(^{176}Hf/^{177}Hf)_{CHUR}$ are the Hf isotope ratio of the zircon and chondritic uniform reservoir (CHUR) at crystallization age, respectively. These values were calculated using the radiogenic equation, the present-day measured $^{176}Hf/^{177}Hf$ and $^{176}Lu/^{177}Hf$, and a radiogenic decay constant of 1.867×10^{-11} years (*305*). $(^{176}Hf/^{177}Hf)_{CHUR}$ and $(^{176}Lu/^{177}Hf)_{CHUR}$ at the present day are 0.282772 ± 29 and 0.0332 ± 2, respectively (*306*). $(^{87}Sr/^{86}Sr)_{CHUR}$ and $(^{87}Rb/^{86}Sr)_{CHUR}$ at the present day are 0.7045 and 0.0824 (*307*, *308*).

Debiasing the detrital zircon record

Debiasing method.

In accordance with the Horvitz-Thompson estimation theory, we used weighted resampling to correct for biases in the detrital zircon record and to obtain the best estimate of the εHf ratio of zircon-bearing igneous rocks. The Horvitz-Thompson estimation theory dictates that an unbiased estimate of εHf at any time can be obtained by weighting each observation with the inverse of its inclusion probability in the sample (*309*). We resampled with replacement (bootstrap) from our database with resample probabilities equal to the Horvitz-Thompson weights and performed a smoothing procedure on the resampled data set to obtain an approximately unbiased estimate of the εHf trend through time. Note that our resampling procedure is similar to that of Keller and Schoene (*31*), although we made the connection between weighting and unbiasedness explicit via the Horvitz-Thompson estimation theory.

We note three key sources of preferential sampling (bias) in our database. First, sediments present in the database integrate different proportions of the Earth's surface. Some sediments in our database drain very large catchment (for example, the Mississippi River), whereas some others represent much smaller catchments. The sediments draining large catchments tend to have a broader U-Pb date distribution than those draining smaller catchments. The zircon grains collected in small catchments are more likely to be biased toward a more local magmatic signature than those in the larger catchments. We did not identify a proper way to correct for this bias, but to minimize it, we used only sediments with Cenozoic and Mesozoic depositional age, which represent 24,715 zircon grains from 535 individual Mesozoic and Cenozoic sediments. The idea is that older zircon grains in those

young sediments likely represent a more integrated picture of Earth's surface because they had time to mix during multiple sedimentary cycles.

Second, a disproportionate number of samples were observed from similar geospatial locations (geographic bias) (fig. S1). If uncorrected, Asian samples would dominate the estimation of trend εHf. We assumed that the present-day sediment geographic distribution was a sufficient estimate for geographic debiasing because of the relatively similar paleogeography throughout this period. We weighted the geographic locations of each sediment sample using

$$w_i^{\mathrm{geo}} = \frac{1}{\mathrm{var}(\mathrm{dist}(i,j))} \quad (2)$$

where dist(*i*,*j*) represents the haversine distance between the location of sediment *i* and the location of sediment *j*, and var denotes the sample variance of the distances.

Third, to correct the bias introduced by a larger number of zircon grains sampled from the same sediment (sampling bias) (fig. S2), we introduced the weighting by

$$w_i^{\mathrm{sed}} = \frac{1}{N_i} \quad (3)$$

where N_i is the number of zircon grains sampled for the sediment *i*. To avoid overweighing poorly sampled sediments, we screened out sediments with less than 10 zircon grains sampled. The final database used during the debiasing procedure contained 24,377 individual zircon grains from 470 individual sediments deposited during the Cenozoic or Mesozoic.

To combine these sampling mechanisms into a resample probability that places equal importance on each mechanism, it is necessary to rescale each component. We chose to do this by matching the first and second sample moments via a location- and scale-preserving correction function, z(·), which ensures that the collection of weights has a mean of 100 and an SD of 10 for each of the two mechanisms. Thus, our overall resample probabilities are given by

$$w_i^{\mathrm{tot}} = z(w_i^{\mathrm{geo}}) + z(w_i^{\mathrm{sed}}) \quad (4)$$

We chose a resample of size 10^6 to balance computational constraints and ensure that actual resampled proportions were approximately equal to the desired resample proportion.

Response of the εHf trend to resampling procedure.

The spatial distribution of geographic weights shows higher weights for isolated samples and lower weights for clustered samples, as we intended our weighted resampling procedure to induce (fig. S3). The prior and posterior density distributions were compared to the present-day distribution of continental surfaces (fig. S4). The results suggest substantial improvement in geographic sampling distribution. However, as observed with the relatively bimodal distribution of the geographic weights (fig. S3), the geographic declustering procedure could benefit from applying more advanced three-dimensional declustering methods. Prior and posterior resampling distributions of zircon U-Pb date as well as secular εHf curve do not change markedly after resampling (fig. S5), although undersampled and isolated samples have a much higher weight (figs. S6 and S7). The U-Pb date distribution of the resampled database resembles the U-Pb date distributions of previous databases, with a series of U-Pb peaks centered on supercontinent periods (fig. S5). However, we used only sediments deposited during the Mesozoic and Cenozoic, which explains the progressive increase in zircon frequency throughout Earth's history that is not observed in other databases compiling sediments of all depositional ages. Previous work also noted that the secular trends in εHf differed between compilations for the last 250 Ma of Earth's history (*46*). We suggest that these differences are associated with significant geographic biases in these databases. The database compiled in this work markedly extends the geographic coverage of Mesozoic and Cenozoic zircon grains. Our debiasing approach also limits the influence of sampling and geographic biases in investigating the resulting εHf trend.

Propagating U-Pb date and εHf uncertainties in the smoothed εHf trend

Gaussian noise resampling.

On the basis of the resampled data set, the εHf trend was calculated using a rolling median or rolling mean at 1 My, chosen to balance smoothness and informativity (Fig. 1). However, although we tried to minimize uncertainty through our screening procedure, both the U-Pb date and εHf value of individual zircon grains contain significant uncertainty. To test the sensitivity of the smoothed εHf trend to these uncertainties, we resampled the debiased data set by introducing Gaussian noise around individual U-Pb and εHf values using a range of uncertainties for each variable. We calculated a median age discordance of 2% (Q1, 0.7%; Q3, 4.1%) using the zircon grains for which the absolute age discordance was compiled (21% of the data). Similarly, we calculated a median uncertainty for εHf values of ±0.62 (Q1, ±0.45; Q3, ±1).

Response to Gaussian noise resampling.

We found that the smoothed εHf trend is mostly sensitive to uncertainty in U-Pb date (fig. S8). The smoothed εHf trend shows very little change when testing a range of uncertainty for the εHf value (fig. S9). Conversely, the overall amplitude of variations decreases progressively as larger U-Pb date discordances are considered (fig. S8). For U-Pb date discordance superior to 10%, the smoothed εHf trend loses most of its structure, suggesting that lower discordance threshold should be considered when trying to reconstruct the long-term evolution of εHf through time (fig. S8). We choose the εHf trend accounting for the median uncertainty in U-Pb date (±2%) and εHf (±0.62) as our reference smoothed curve (Fig. 1).

Normalized $(^{87}Sr/^{86}Sr)_{seawater}$ curves

We used existing compilations of $^{87}Sr/^{86}Sr$ analysis in carbonates to generate the $(^{87}Sr/^{86}Sr)_{seawater}$ ratio curve over the last 850 My (*13*, *15*). The quality and uncertainty associated with these data vary (*310*). The age model of Phanerozoic carbonates is usually more precise (<1 Ma) than that of Proterozoic carbonates (>5 Ma). The sampling density is much higher in the Cenozoic and Mesozoic and decreases progressively with time because of the scarcity of exposed carbonates with ages older than the Mesozoic (fig. S10). The sampling density remains higher than 1 My for the entire Phanerozoic, whereas several data gaps exist throughout the Ediacaran and Cryogenian. This low sampling density complicates the comparison of the Proterozoic trend with the $(^{87}Sr/^{86}Sr)_{i\text{-}zig}$ ratio. We applied a linear resampling to fill data gaps in the Proterozoic and calculated the median $(^{87}Sr/^{86}Sr)_{seawater}$ ratio at a 1-My time step.

To facilitate the time series analysis between $(^{87}Sr/^{86}Sr)_{seawater}$ and $(^{87}Sr/^{86}Sr)_{i\text{-}zig}$ curves, we detrended the $(^{87}Sr/^{86}Sr)_{seawater}$ variations $[N(^{87}Sr/^{86}Sr)_{seawater}]$. $(^{87}Sr/^{86}Sr)_{seawater}$ ratio displays an exponential increase throughout Earth's history primarily driven by the radiogenic decay of ^{87}Rb into ^{86}Sr in the silicate crust (*12*). On the basis of the radiogenic equation, the rate of radiogenic decay through time is controlled by the Rb/Sr ratio of the silicate crust. Rb and Sr are incompatible elements and are progressively concentrated into crustal silicates throughout Earth's history, leaving the mantle depleted in these elements. Rb, being less compatible than Sr, further concentrates into crustal silicates, which leads to an increase in the Rb/Sr ratio of the crust through time. If the rate of crustal growth was constant throughout Earth's history, the Rb/Sr ratio of crustal silicates would exponentially increase as a mirror image of the Rb/Sr ratio of the depleted mantle, but with a steeper gradient due to the small volume of the crust in comparison with the mantle (*12*). However, the rate of crustal growth was not constant through time and altered this idealistic model (*35*). On the basis of geochemical reconstructions, the time-integrated $^{87}Rb/^{86}Sr$ ratio could have remained relatively constant (*47*) or increased slightly (*31*). Consequently, instead of using an idealized growth curve with a continuous enrichment of the crust (*47*), we used a constant time-integrated $^{87}Rb/^{86}Sr$ ratio for silicates over the last 1000 My as our reference curve. However, we also tested the sensitivity of our conclusions to a potential twofold increase or decrease of the time-integrated $^{87}Rb/^{86}Sr$ ratio. We calculated the evolution of $^{87}Sr/^{86}Sr$ ratio in seawater associated with radiogenic decay over the last 1000 Ma as

$$\left(\frac{^{87}Sr}{^{86}Sr}(t)\right)_{seawater\text{-}decay} = \left(\frac{^{87}Sr}{^{86}Sr}(t_{1000My})\right)_{seawater} + \left(\frac{^{87}Rb}{^{86}Sr}\right)_{cs}(e^{\lambda t}-1) \quad (5)$$

where $[^{87}Sr/^{86}Sr(t)]_{seawater\text{-}decay}$ is the $^{87}Sr/^{86}Sr$ ratio of seawater associated with radiogenic decay through time, $[^{87}Sr/^{86}Sr(t_{1000\ My})]_{seawater}$ is the $^{87}Sr/^{86}Sr$ of seawater at t = 1000 My, $(^{87}Rb/^{86}Sr)_{cs}$ is the $^{87}Rb/^{86}Sr$ of the crust silicates for the last 1000 My, and λ is the decay constant of the parent isotope (1.42×10^{-11} $year^{-1}$).

$N(^{87}Sr/^{86}Sr)_{seawater}$ is calculated as

$$N\left(\frac{^{87}Sr}{^{86}Sr}(t)\right)_{seawater} = \left(\frac{^{87}Sr}{^{86}Sr}(t)\right)_{seawater} - \left(\frac{^{87}Sr}{^{86}Sr}(t)\right)_{seawater\text{-}decay} \quad (6)$$

We calculated the present-day value of the time-integrated $^{87}Rb/^{86}Sr$ ratio of the continental crust as

$$\left(\frac{^{87}Sr}{^{86}Sr}\right)_{riverine} = \left(\frac{^{87}Sr}{^{86}Sr}\right)_{cs} f_{cs} + \left(\frac{^{87}Sr}{^{86}Sr}\right)_{carb} f_{carb}$$

$$\left(\frac{^{87}Sr}{^{86}Sr}\right)_{cs} = \frac{\left(\frac{^{87}Sr}{^{86}Sr}\right)_{riverine} - \left(\frac{^{87}Sr}{^{86}Sr}\right)_{carb} f_{carb}}{f_{cs}} \quad (7)$$

where $(^{87}Sr/^{86}Sr)_{riverine}$ ratio is the $^{87}Sr/^{86}Sr$ ratio of the Sr exported from rivers at the present day (0.71144) (*311*, *312*); $(^{87}Sr/^{86}Sr)_{crust}$ and $(^{87}Sr/^{86}Sr)_{carb}$ are the $^{87}Sr/^{86}Sr$ ratio of the continental crust silicates and carbonates, respectively, with $(^{87}Sr/^{86}Sr)_{carb}$ equal to 0.708 at the present day (*52*, *311*, *313*); and f_{cs} and f_{carb} are the relative fluxes of Sr from the continental crust silicates and carbonates at the present day (0.37 and 0.63, respectively) (*52*, *311*, *313*).

$$\left(\frac{^{87}Rb}{^{86}Sr}\right)_{cs} = \frac{\left(\frac{^{87}Sr}{^{86}Sr}\right)_{cs} - \left(\frac{^{87}Sr}{^{86}Sr}\right)_{i}}{(e^{\lambda t}-1)} \quad (8)$$

where λ is the decay constant of the parent isotope (1.42×10^{-11} $year^{-1}$) and $(^{87}Sr/^{86}Sr)_i$ is the initial $^{87}Sr/^{86}Sr$ of the bulk silicate Earth 4550 Ma (0.69897) (*307*).

We applied Eq. (7) and found a $^{87}Sr/^{86}Sr$ ratio of continental crust silicates of 0.7178 at the present day, with a corresponding $^{8}Rb/^{86}Sr$ ratio of silicates of 0.283. This value is used in Eqs. (6) and (7) to calculate the $N(^{87}Sr/^{86}Sr)_{seawater}$ ratio.

Time-series analysis

Both $(^{87}Sr/^{86}Sr)_{seawater}$ and $(^{87}Sr/^{86}Sr)_{i\text{-}zig}$ curves have been decomposed into a slow-varying trend component and a fast-varying component by applying two respective fourth-order Butterworth filters. A Butterworth filter is a widely used technique to decompose a time series into components with a given periodicity range. The slow-varying component was isolated from the original record by using a cutoff corner frequency at 1/700 My^{-1} with a low-pass Butterworth filter. The filter results in a slow-varying component that has a time scale of 700 My or longer. The fast-varying component was calculated using a band-pass Butterworth filter with a cutoff frequency between 1/700 and 1/30 My^{-1}. These cutoff frequencies were selected so that the half periodicity covers the range of subduction and orogeny durations during Earth's history (*46*). Cross-correlation coefficient analysis was applied to investigate the potential linear dependence between the pair of slow-varying components and also that between the pair of fast-varying components. In addition to correlation coefficient, which shows the linear dependence between two time series, the cross-correlation can further reveal possible lead-lag relationship, which depends on the sign of lag that corresponds to the maximum coefficient.

Sensitivity analysis

In the first step, we verified whether the smoothed $(^{87}Sr/^{86}Sr)_{i\text{-}zig}$ trend holds for different debiasing and resampling procedures. This is an important question considering the scatter in εHf values (fig. S5). We have already shown that the smoothed εHf trend [hence, the $(^{87}Sr/^{86}Sr)_{i\text{-}zig}$ ratio] is sensitive to the uncertainty in U-Pb date (fig. S8) but not sensitive to the uncertainty in εHf value. We further tested the sensitivity of the time series analysis to our screening and debiasing procedures. In the first simulation, we tested the impact of our debiasing procedure choices. We changed the sampling weight calculation from $1/n$ to $1/n^2$. The resulting smoothed $(^{87}Sr/^{86}Sr)_{i\text{-}zig}$ ratio and the time series analysis show almost no difference with our reference case (Fig. 3 and fig. S11). In the second simulation, we tested the sensitivity of our screening procedure to the time series analysis. Instead of using a data set with only sediments with Cenozoic and Mesozoic depositional ages, we used a data set with sediment of all depositional ages. We applied the same screening and debiasing procedure as in our reference case. In this scenario, the resulting smoothed $(^{87}Sr/^{86}Sr)_{i\text{-}zig}$ ratio shows some significant differences with our reference data set (Fig. 3 and fig. S12). The correlation between the time series is slightly lower than in our reference

case, but the conclusions remain unchanged: The CCF between the two time series remains significant and centered on zero (fig. S12). We suggest that the slight decrease in correlation observed in this scenario reflects the integration of zircon data from small rivers that oversample local magmatism and bias the smoothed εHf values.

In the second step, we tested the sensitivity of the time series analysis when using a range of calibration procedures for the $N(^{87}Sr/^{86}Sr)_{seawater}$ ratio. In the first scenario, we assumed that the time-integrated $^{87}Rb/^{86}Sr$ ratio increased, following an ideal growth model increasing by a factor of 2 throughout the last 1000 Ma (fig. S13) (*310*). In the second scenario, we assumed that the time-integrated $^{87}Rb/^{86}Sr$ ratio decreased by a factor of 2 throughout the last 1000 Ma (fig. S14) (*47*). The modifications in the parameterization of the time-integrated $^{87}Rb/^{86}Sr$ ratio calibration lead to some significant changes in the slow-varying trend of $(^{87}Sr/^{86}Sr)_{i\text{-}zig}$ ratio but changes little the fast-varying $(^{87}Sr/^{86}Sr)_{i\text{-}zig}$ trend. In both scenarios, the correlation between $(^{87}Sr/^{86}Sr)_{i\text{-}zig}$ ratio and $N(^{87}Sr/^{86}Sr)_{seawater}$ ratio remains significant and centered on zero (figs. S12 and S13).

SUPPLEMENTARY MATERIALS

Supplementary material for this article is available at http://advances.sciencemag.org/cgi/content/full/3/3/e1602183/DC1

fig. S1. Map of sediment locations.
fig. S2. Sampling bias: Histogram of zircon grain count per sediment from the screened data set (24,377 individual zircon grains from 470 individual sediments).
fig. S3. Geographic bias and geographic weights: Map of sediment sample locations for the screened data set with associated geographic resampling weights.
fig. S4. Geographic debiasing validation.
fig. S5. Resampled εHf using combined weights (red) superimposed on nonresampled εHf (black) from detrital zircons from Cenozoic and Mesozoic sediment data compiled in database S1.
fig. S6. Map of sediment sample locations with associated final resampling weights combining geographic and sampling weights.
fig. S7. Resampling weights visualization.
fig. S8. Sensitivity of the smoothed εHf trend to the uncertainty in U-Pb date.
fig. S9. Sensitivity of the smoothed εHf trend to the uncertainty in εHf values.
fig. S10. Evolution of the $(^{87}Sr/^{86}Sr)_{seawater}$ ratio in the last 1000 My from the analysis of $^{87}Sr/^{86}Sr$ ratio of carbonates.
fig. S11. Sensitivity of time series analysis to debiasing procedures.
fig. S12. Sensitivity of time series analysis to data screening.
fig. S13. Sensitivity of time series analysis to $N(^{87}Sr/^{86}Sr)_{seawater}$ curve parameterization by assuming a linear increase in Rb/Sr ratio of the crust in the last 1000 My.
fig. S14. Sensitivity of time series analysis to $N(^{87}Sr/^{86}Sr)_{seawater}$ curve parameterization by assuming a linear decrease in Rb/Sr ratio of the crust in the last 1000 My.
database S1. Excel data table with worldwide U-Pb and Hf isotopes in detrital zircons compiled from the literature.
database S2. Excel data table with $^{87}Sr/^{86}Sr$ and $^{143}Nd/^{144}Nd$ ratio data from whole igneous rock and U-Pb and Hf isotope data from their hosted zircons compiled from the literature.

REFERENCES AND NOTES

1. J. C. G. Walker, P. B. Hays, J. F. Kasting, A negative feedback mechanism for the long-term stabilization of Earth's surface temperature. *J. Geophys. Res. Oceans* **86**, 9776–9782 (1981).
2. L. R. Kump, S. L. Brantley, M. A. Arthur, Chemical weathering, atmospheric CO_2, and climate. *Annu. Rev. Earth Planet. Sci.* **28**, 611–667 (2000).
3. M. E. Raymo, W. F. Ruddiman, P. N. Froelich, Influence of late Cenozoic mountain building on ocean geochemical cycles. *Geology* **16**, 649–653 (1988).
4. A. J. West, A. Galy, M. Bickle, Tectonic and climatic controls on silicate weathering. *Earth Planet. Sci. Lett.* **235**, 211–228 (2005).
5. Y. Goddéris, Y. Donnadieu, G. Le Hir, V. Lefebvre, E. Nardin, The role of palaeogeography in the Phanerozoic history of atmospheric CO_2 and climate. *Earth Sci. Rev.* **128**, 122–138 (2014).
6. R. A. Berner, A model for atmospheric CO_2 over Phanerozoic time. *Am. J. Sci.* **291**, 339–376 (1991).
7. J. C. Zachos, B. N. Opdyke, T. M. Quinn, C. E. Jones, A. N. Halliday, Early cenozoic glaciation, Antarctic weathering, and seawater $^{87}Sr/^{86}Sr$: Is there a link? *Chem. Geol.* **161**, 165–180 (1999).
8. D. J. Beerling, R. A. Berner, Feedbacks and the coevolution of plants and atmospheric CO_2. *Proc. Natl. Acad. Sci. U.S.A.* **102**, 1302–1305 (2005).
9. R. A. Berner, GEOCARBSULF: A combined model for Phanerozoic atmospheric O_2 and CO_2. *Geochim. Cosmochim. Acta* **70**, 5653–5664 (2006).
10. Y. Goddéris, L. M. François, A. Probst, J. Schott, D. Moncoulon, D. Labat, D. Viville, Modelling weathering processes at the catchment scale: The WITCH numerical model. *Geochim. Cosmochim. Acta* **70**, 1128–1147 (2006).
11. J. Veizer, Strontium isotopes in seawater through time. *Annu. Rev. Earth Planet. Sci.* **17**, 141–167 (1989).
12. G. A. Shields, A normalised seawater strontium isotope curve and the Neoproterozoic-Cambrian chemical weathering event. *eEarth Discuss.* **2**, 69–84 (2007).
13. J. Veizer, D. Ala, K. Azmy, P. Bruckschen, D. Buhl, F. Bruhn, G. A. F. Carden, A. Diener, S. Ebneth, Y. Godderis, T. Jasper, C. Korte, F. Pawellek, O. G. Podlaha, H. Strauss, $^{87}Sr/^{86}Sr$, $\delta^{13}C$ and $\delta^{18}O$ evolution of Phanerozoic seawater. *Chem. Geol.* **161**, 59–88 (1999).
14. G. W. Brass, The variation of the marine $^{87}Sr^{86}Sr$ ratio during Phanerozonic time: Interpretation using a flux model. *Geochim. Cosmochim. Acta* **40**, 721–730 (1976).
15. G. P. Halverson, F. Ö. Dudás, A. C. Maloof, S. A. Bowring, Evolution of the $^{87}Sr/^{86}Sr$ composition of Neoproterozoic seawater. *Palaeogeogr. Palaeoclimatol. Palaeoecol.* **256**, 103–129 (2007).
16. F. M. Richter, D. B. Rowley, D. J. Depaolo, Sr isotope evolution of seawater: The role of tectonics. *Earth Planet. Sci. Lett.* **109**, 11–23 (1992).
17. M. R. Palmer, H. Elderfield, Sr isotope composition of sea water over the past 75 Myr. *Nature* **314**, 526–528 (1985).
18. R. L. Armstrong, Glacial erosion and the variable isotopic composition of strontium in seawater. *Nature* **230**, 132–133 (1971).
19. D. G. Van Der Meer, R. E. Zeebe, D. J. J. van Hinsbergen, A. Sluijs, W. Spakman, T. H. Torsvik, Plate tectonic controls on atmospheric CO_2 levels since the Triassic. *Proc. Natl. Acad. Sci. U.S.A.* **111**, 4380–4385 (2014).
20. L. A. Coogan, S. E. Dosso, Alteration of ocean crust provides a strong temperature dependent feedback on the geological carbon cycle and is a primary driver of the Sr-isotopic composition of seawater. *Earth Planet. Sci. Lett.* **415**, 38–46 (2015).
21. A. Prokoph, H. El Bilali, R. Ernst, Periodicities in the emplacement of large igneous provinces through the Phanerozoic: Relations to ocean chemistry and marine biodiversity evolution. *Geosci. Front.* **4**, 263–276 (2013).
22. O. Jagoutz, F. A. Macdonald, L. Royden, Low-latitude arc–continent collision as a driver for global cooling. *Proc. Natl. Acad. Sci. U.S.A.* **113**, 4935–4940 (2016).
23. G. M. Cox, G. P. Halverson, R. K. Stevenson, M. Vokaty, A. Poirier, M. Kunzmann, Z.-X. Li, S. W. Denyszyn, J. V. Strauss, F. A. Macdonald, Continental flood basalt weathering as a trigger for Neoproterozoic Snowball Earth. *Earth Planet. Sci. Lett.* **446**, 89–99 (2016).
24. J. D. Blum, C. A. Gazis, A. D. Jacobson, C. Page Chamberlain, Carbonate versus silicate weathering in the Raikhot watershed within the High Himalayan Crystalline Series. *Geology* **26**, 411–414 (1998).
25. A. Galy, C. France-Lanord, L. A. Derry, The strontium isotopic budget of Himalayan rivers in Nepal and Bangladesh. *Geochim. Cosmochim. Acta* **63**, 1905–1925 (1999).
26. J. P. Davidson, R. J. Arculus, The significance of Phanerozoic arc magmatism in generating continental crust, in *Evolution and Differentiation of the Continental Crust,* T. Rushmer, M. Brown, Eds. (Cambridge Univ. Press, 2006), pp. 135–172.
27. P. A. Cawood, C. J. Hawkesworth, B. Dhuime, The continental record and the generation of continental crust. *Geol. Soc. Am. Bull.* **125**, 14–32 (2013).
28. N. R. McKenzie, B. K. Horton, S. E. Loomis, D. F. Stockli, N. J. Planavsky, C.-T. A. Lee, Continental arc volcanism as the principal driver of icehouse-greenhouse variability. *Science* **352**, 444–447 (2016).
29. C. P. Bataille, G. J. Bowen, Mapping $^{87}Sr/^{86}Sr$ variations in bedrock and water for large scale provenance studies. *Chem. Geol.* **304–305**, 39–52 (2012).
30. C. P. Bataille, S. R. Brennan, J. Hartmann, N. Moosdorf, M. J. Wooller, G. J. Bowen, A geostatistical framework for predicting variations in strontium concentrations and isotope ratios in Alaskan rivers. *Chem. Geol.* **389**, 1–15 (2014).
31. C. B. Keller, B. Schoene, Statistical geochemistry reveals disruption in secular lithospheric evolution about 2.5 Gyr ago. *Nature* **485**, 490–493 (2012).
32. G. Gehrels, Detrital zircon U-Pb geochronology applied to tectonics. *Annu. Rev. Earth Planet. Sci.* **42**, 127–149 (2014).
33. K. C. Condie, M. E. Bickford, R. C. Aster, E. Belousova, D. W. Scholl, Episodic zircon ages, Hf isotopic composition, and the preservation rate of continental crust. *Geol. Soc. Am. Bull.* **123**, 951–957 (2011).
34. B. Dhuime, C. J. Hawkesworth, P. A. Cawood, C. D. Storey, A change in the geodynamics of continental growth 3 billion years ago. *Science* **335**, 1334–1336 (2012).

35. N. M. W. Roberts, C. J. Spencer, The zircon archive of continent formation through time. *Geol. Soc. Spec. Publ.* **389**, 197–225 (2015).
36. E. A. Belousova, Y. A. Kostitsyn, W. L. Griffin, G. C. Begg, S. Y. O'Reilly, N. J. Pearson, The growth of the continental crust: Constraints from zircon Hf-isotope data. *Lithos* **119**, 457–466 (2010).
37. C.-T. A. Lee, L. Y. Yeung, N. R. McKenzie, Y. Yokoyama, K. Ozaki, A. Lenardic, Two-step rise of atmospheric oxygen linked to the growth of continents. *Nat. Geosci.* **9**, 417–424 (2016).
38. S. E. Bryan, L. Ferrari, Large igneous provinces and silicic large igneous provinces: Progress in our understanding over the last 25 years. *Geol. Soc. Am. Bull.* **125**, 1053–1078 (2013).
39. K. Condie, Preservation and recycling of crust during accretionary and collisional phases of Proterozoic orogens: A bumpy road from Nuna to Rodinia. *Geosciences* **3**, 240–261 (2013).
40. C. J. Hawkesworth, B. Dhuime, A. B. Pietranik, P. A. Cawood, A. I. S. Kemp, C. D. Storey, The generation and evolution of the continental crust. *J. Geol. Soc.* **167**, 229–248 (2010).
41. C. Hawkesworth, P. Cawood, T. Kemp, C. Storey, B. Dhuime, A matter of preservation. *Science* **323**, 49–50 (2009).
42. P. A. Cawood, C. J. Hawkesworth, B. Dhuime, Detrital zircon record and tectonic setting. *Geology* **40**, 875–878 (2012).
43. C. J. Spencer, P. A. Cawood, C. J. Hawkesworth, A. R. Prave, N. M. W. Roberts, M. S. A. Horstwood, M. J. Whitehouse; EIMF, Generation and preservation of continental crust in the Grenville Orogeny. *Geosci. Front.* **6**, 357–372 (2015).
44. K. C. Condie, Growth of continental crust: A balance between preservation and recycling. *Mineral. Mag.* **78**, 623–637 (2014).
45. G. Faure, *Origin of Igneous Rocks: The Isotopic Evidence* (Springer, 2001).
46. K. C. Condie, R. C. Aster, Refinement of the supercontinent cycle with Hf, Nd and Sr isotopes. *Geosci. Front.* **4**, 667–680 (2013).
47. B. Dhuime, A. Wuestefeld, C. J. Hawkesworth, Emergence of modern continental crust about 3 billion years ago. *Nat. Geosci.* **8**, 552–555 (2015).
48. W. J. Collins, E. A. Belousova, A. I. S. Kemp, J. B. Murphy, Two contrasting Phanerozoic orogenic systems revealed by hafnium isotope data. *Nat. Geosci.* **4**, 333–337 (2011).
49. J. Hartmann, N. Moosdorf, The new global lithological map database GLiM: A representation of rock properties at the Earth surface. *Geochem. Geophys. Geosyst.* **13**, Q12004 (2012).
50. C. Dessert, B. Dupré, J. Gaillardet, L. M. François, C. J. Allègre, Basalt weathering laws and the impact of basalt weathering on the global carbon cycle. *Chem. Geol.* **202**, 257–273 (2003).
51. A. S. Taylor, A. C. Lasaga, The role of basalt weathering in the Sr isotope budget of the oceans. *Chem. Geol.* **161**, 199–214 (1999).
52. C.-J. Allegre, P. Louvat, J. Gaillardet, L. Meynadier, S. Rad, F. Capmas, The fundamental role of island arc weathering in the oceanic Sr isotope budget. *Earth Planet. Sci. Lett.* **292**, 51–56 (2010).
53. K. Fiege, C. A. Miller, L. F. Robinson, R. Figueroa, B. Peucker-Ehrenbrink, Strontium isotopes in Chilean rivers: The flux of unradiogenic continental Sr to seawater. *Chem. Geol.* **268**, 337–343 (2009).
54. P. Bird, An updated digital model of plate boundaries. *Geochem. Geophys. Geosyst.* **4**, 1027 (2003).
55. D. B. Rowley, Rate of plate creation and destruction: 180 Ma to present. *Geol. Soc. Am. Bull.* **114**, 927–933 (2002).
56. Y. Goddéris, G. Le Hir, M. Macouin, Y. Donnadieu, L. Hubert-Théou, G. Dera, M. Aretz, F. Fluteau, Z. X. Li, G. P. Halverson, Paleogeographic forcing of the strontium isotopic cycle in the Neoproterozoic. *Gondwana Res.* **42**, 151–162 (2017).
57. C. Korte, T. Jasper, H. W. Kozur, J. Veizer, $^{87}Sr/^{86}Sr$ record of Permian seawater. *Palaeogeogr. Palaeoclimatol. Palaeoecol.* **240**, 89–107 (2006).
58. C. J. Spencer, C. Hawkesworth, P. A. Cawood, B. Dhuime, Not all supercontinents are created equal: Gondwana-Rodinia case study. *Geology* **41**, 795–798 (2013).
59. J. M. Batumike, S. Y. O'Reilly, W. L. Griffin, E. A. Belousova, U–Pb and Hf-isotope analyses of zircon from the Kundelungu Kimberlites, D.R. Congo: Implications for crustal evolution. *Precambrian Res.* **156**, 195–225 (2007).
60. E. A. Belousova, A. J. Reid, W. L. Griffin, S. Y. O'Reilly, Rejuvenation vs. recycling of Archean crust in the Gawler Craton, South Australia: Evidence from U–Pb and Hf isotopes in detrital zircon. *Lithos* **113**, 570–582 (2009).
61. K. C. Condie, E. Beyer, E. Belousova, W. L. Griffin, S. Y. O'Reilly, U–Pb isotopic ages and Hf isotopic composition of single zircons: The search for juvenile Precambrian continental crust. *Precambrian Res.* **139**, 42–100 (2005).
62. B. Dhuime, C. J. Hawkesworth, C. D. Storey, P. A. Cawood, From sediments to their source rocks: Hf and Nd isotopes in recent river sediments. *Geology* **39**, 407–410 (2011).
63. W. L. Griffin, E. A. Belousova, S. R. Shee, N. J. Pearson, S. Y. O'Reilly, Archean crustal evolution in the northern Yilgarn Craton: U–Pb and Hf-isotope evidence from detrital zircons. *Precambrian Res.* **131**, 231–282 (2004).
64. L. van Hoang, F.-Y. Wu, P. D. Clift, A. Wysocka, A. Swierczewska, Evaluating the evolution of the Red River system based on in situ U-Pb dating and Hf isotope analysis of zircons. *Geochem. Geophys. Geosyst.* **10**, Q11008 (2009).
65. T. Iizuka, T. Komiya, S. Rino, S. Maruyama, T. Hirata, Detrital zircon evidence for Hf isotopic evolution of granitoid crust and continental growth. *Geochim. Cosmochim. Acta* **74**, 2450–2472 (2010).
66. A. I. S. Kemp, G. L. Foster, A. Scherstén, M. J. Whitehouse, J. Darling, C. Storey, Concurrent Pb–Hf isotope analysis of zircon by laser ablation multi-collector ICP-MS, with implications for the crustal evolution of Greenland and the Himalayas. *Chem. Geol.* **261**, 244–260 (2009).
67. F. Meng, S. Gao, H. Yuan, H. Gong, Permian-Triassic (260-220 Ma) crustal growth of Eastern Central Asian orogenic belt as revealed by detrital zircon studies. *Am. J. Sci.* **310**, 364–404 (2010).
68. A. Mišković, U. Schaltegger, Crustal growth along a non-collisional cratonic margin: A Lu–Hf isotopic survey of the Eastern Cordilleran granitoids of Peru. *Earth Planet. Sci. Lett.* **279**, 303–315 (2009).
69. V. Murgulov, E. Beyer, W. L. Griffin, S. Y. O'Reilly, S. G. Walters, D. Stephens, Crustal evolution in the Georgetown Inlier, North Queensland, Australia: A detrital zircon grain study. *Chem. Geol.* **245**, 198–218 (2007).
70. V. Ravikant, F.-Y. Wu, W.-Q. Ji, U–Pb age and Hf isotopic constraints of detrital zircons from the Himalayan foreland Subathu sub-basin on the Tertiary palaeogeography of the Himalaya. *Earth Planet. Sci. Lett.* **304**, 356–368 (2011).
71. I. Sevastjanova, B. Clements, R. Hall, E. A. Belousova, W. L. Griffin, N. Pearson, Granitic magmatism, basement ages, and provenance indicators in the Malay Peninsula: Insights from detrital zircon U–Pb and Hf-isotope data. *Gondwana Res.* **19**, 1024–1039 (2011).
72. M. Tunik, A. Folguera, M. Naipauer, M. Pimentel, V. A. Ramos, Early uplift and orogenic deformation in the Neuquén Basin: Constraints on the Andean uplift from U–Pb and Hf isotopic data of detrital zircons. *Tectonophysics* **489**, 258–273 (2010).
73. T. Usuki, C.-Y. Lan, K.-L. Wang, H.-Y. Chiu, Linking the Indochina block and Gondwana during the Early Paleozoic: Evidence from U–Pb ages and Hf isotopes of detrital zircons. *Tectonophysics* **586**, 145–159 (2013).
74. J. J. Veevers, A. Saeed, Permian–Jurassic Mahanadi and Pranhita–Godavari Rifts of Gondwana India: Provenance from regional paleoslope and U–Pb/Hf analysis of detrital zircons. *Gondwana Res.* **16**, 633–654 (2009).
75. J. J. Veevers, E. A. Belousova, A. Saeed, K. Sircombe, A. F. Cooper, S. E. Read, Pan-Gondwanaland detrital zircons from Australia analysed for Hf-isotopes and trace elements reflect an ice-covered Antarctic provenance of 700–500 Ma age, T_{DM} of 2.0–1.0 Ga, and alkaline affinity. *Earth Sci. Rev.* **76**, 135–174 (2006).
76. J. J. Veevers, A. Saeed, P. E. O'Brien, Provenance of the Gamburtsev Subglacial Mountains from U–Pb and Hf analysis of detrital zircons in Cretaceous to Quaternary sediments in Prydz Bay and beneath the Amery Ice Shelf. *Sediment. Geol.* **211**, 12–32 (2008).
77. C. Y. Wang, I. H. Campbell, C. M. Allen, I. S. Williams, S. M. Eggins, Rate of growth of the preserved North American continental crust: Evidence from Hf and O isotopes in Mississippi detrital zircons. *Geochim. Cosmochim. Acta* **73**, 712–728 (2009).
78. F.-Y. Wu, J.-H. Yang, S. A. Wilde, X.-M. Liu, J.-H. Guo, M.-G. Zhai, Detrital zircon U–Pb and Hf isotopic constraints on the crustal evolution of North Korea. *Precambrian Res.* **159**, 155–177 (2007).
79. F.-Y. Wu, P. D. Clift, J.-H. Yang, Zircon Hf isotopic constraints on the sources of the Indus Molasse, Ladakh Himalaya, India. *Tectonics* **26**, TC2014 (2007).
80. F.-Y. Wu, W.-Q. Ji, C.-Z. Liu, S.-L. Chung, Detrital zircon U–Pb and Hf isotopic data from the Xigaze fore-arc basin: Constraints on Transhimalayan magmatic evolution in southern Tibet. *Chem. Geol.* **271**, 13–25 (2010).
81. J. Yang, S. Gao, C. Chen, Y. Tang, H. Yuan, H. Gong, S. Xie, J. Wang, Episodic crustal growth of North China as revealed by U–Pb age and Hf isotopes of detrital zircons from modern rivers. *Geochim. Cosmochim. Acta* **73**, 2660–2673 (2009).
82. J.-H. Yang, F.-Y. Wu, J.-A. Shao, S. A. Wilde, L.-W. Xie, X.-M. Liu, Constraints on the timing of uplift of the Yanshan Fold and Thrust Belt, North China. *Earth Planet. Sci. Lett.* **246**, 336–352 (2006).
83. C. Y. Wang, I. H. Campbell, A. S. Stepanov, C. M. Allen, I. N. Burtsev, Growth rate of the preserved continental crust: II. Constraints from Hf and O isotopes in detrital zircons from Greater Russian Rivers. *Geochim. Cosmochim. Acta* **75**, 1308–1345 (2011).
84. T. Andersen, M. Elburg, A. Cawthorn-Blazeby, U–Pb and Lu–Hf zircon data in young sediments reflect sedimentary recycling in eastern South Africa. *J. Geol. Soc.* **173**, 337–351 (2016).
85. Y. Xu, C. Y. Wang, T. Zhao, Using detrital zircons from river sands to constrain major tectono-thermal events of the Cathaysia Block, SE China. *J. Asian Earth Sci.* **124**, 1–13 (2016).
86. S. E. Cina, A. Yin, M. Grove, C. S. Dubey, D. P. Shukla, O. M. Lovera, T. K. Kelty, G. E. Gehrels, D. A. Foster, Gangdese arc detritus within the eastern Himalayan Neogene foreland

basin: Implications for the Neogene evolution of the Yalu–Brahmaputra River system. *Earth Planet. Sci. Lett.* **285**, 150–162 (2009).
87. W. L. Griffin, E. A. Belousova, S. G. Walters, S. Y. O'Reilly, Archaean and Proterozoic crustal evolution in the Eastern Succession of the Mt Isa district, Australia: U – Pb and Hf-isotope studies of detrital zircons. *Aust. J. Earth Sci.* **53**, 125–149 (2006).
88. J. Y. Zhang, A. Yin, W. C. Liu, F. Y. Wu, D. Lin, M. Grove, Coupled U-Pb dating and Hf isotopic analysis of detrital zircon of modern river sand from the Yalu River (Yarlung Tsangpo) drainage system in southern Tibet: Constraints on the transport processes and evolution of Himalayan rivers. *Geol. Soc. Am. Bull.* **124**, 9–10 (2012).
89. J. Lloyd, A. S. Collins, J. L. Payne, S. Glorie, S. Holford, A. J. Reid, Tracking the Cretaceous transcontinental Ceduna River through Australia: The hafnium isotope record of detrital zircons from offshore southern Australia. *Geosci. Front.* **7**, 237–244 (2016).
90. T. Iizuka, I. H. Campbell, C. M. Allen, J. B. Gill, S. Maruyama, F. Makoka, Evolution of the African continental crust as recorded by U–Pb, Lu–Hf and O isotopes in detrital zircons from modern rivers. *Geochim. Cosmochim. Acta* **107**, 96–120 (2013).
91. Y. Be'eri-Shlevin, D. Avigad, A. Gerdes, O. Zlatkin, Detrital zircon U–Pb–Hf systematics of Israeli coastal sands: New perspectives on the provenance of Nile sediments. *J. Geol. Soc.* **171**, 107–116 (2013).
92. M. Pepper, G. Gehrels, A. Pullen, M. Ibanez-Mejia, K. M. Ward, P. Kapp, Magmatic history and crustal genesis of western South America: Constraints from U-Pb ages and Hf isotopes of detrital zircons in modern rivers. *Geosphere* **12**, 1532–1555 (2016).
93. M. Pepper, Available from ProQuest Dissertations & Theses Global (1654446666) (2014).
94. G. Gehrels, M. Pecha, Detrital zircon U-Pb geochronology and Hf isotope geochemistry of Paleozoic and Triassic passive margin strata of western North America. *Geosphere* **10**, 49–65 (2014).
95. T. S. RØhr, T. Andersen, H. Dypvik, Provenance of Lower Cretaceous sediments in the Wandel Sea Basin, North Greenland. *J. Geol. Soc.* **165**, 755–767 (2008).
96. T. Ustaömer, P. A. Ustaömer, A. H. F. Robertson, A. Gerdes, Implications of U–Pb and Lu–Hf isotopic analysis of detrital zircons for the depositional age, provenance and tectonic setting of the Permian–Triassic Palaeotethyan Karakaya Complex, NW Turkey. *Int. J. Earth Sci.* **105**, 7–38 (2016).
97. K. D. Surpless, Hornbrook Formation, Oregon and California: A sedimentary record of the Late Cretaceous Sierran magmatic flare-up event. *Geosphere* **11**, 1770–1789 (2015).
98. K. D. Surpless, E. J. Beverly, Understanding a critical basinal link in Cretaceous Cordilleran paleogeography: Detailed provenance of the Hornbrook Formation, Oregon and California. *Geol. Soc. Am. Bull.* **125**, 709–727 (2013).
99. Y. Zhang, D. Jia, L. Shen, H. Yin, Z. Chen, H. Li, Z. Li, C. Sun, Provenance of detrital zircons in the Late Triassic Sichuan foreland basin: Constraints on the evolution of the Qinling Orogen and Longmen Shan thrust-fold belt in central China. *Int. Geol. Rev.* **57**, 1806–1824 (2015).
100. Y.-X. Zhang, X.-C. Tang, K.-J. Zhang, L. Zeng, C.-L. Gao, U–Pb and Lu–Hf isotope systematics of detrital zircons from the Songpan–Ganzi Triassic flysch, NE Tibetan Plateau: Implications for provenance and crustal growth. *Int. Geol. Rev.* **56**, 29–56 (2014).
101. I. Yokelson, G. E. Gehrels, M. Pecha, D. Giesler, C. White, W. C. McClelland, U-Pb and Hf isotope analysis of detrital zircons from Mesozoic strata of the Gravina belt, southeast Alaska. *Tectonics* **34**, 2052–2066 (2015).
102. B. Carrapa, F. S. Mustapha, M. Cosca, G. Gehrels, L. M. Schoenbohm, E. R. Sobel, P. G. DeCelles, J. Russell, P. Goodman, Multisystem dating of modern river detritus from Tajikistan and China: Implications for crustal evolution and exhumation of the Pamir. *Lithosphere* **6**, 443–455 (2014).
103. B.-Q. Wang, W. Wang, W. T. Chen, J.-F. Gao, X.-F. Zhao, D.-P. Yan, M.-F. Zhou, Constraints of detrital zircon U–Pb ages and Hf isotopes on the provenance of the Triassic Yidun Group and tectonic evolution of the Yidun Terrane, Eastern Tibet. *Sediment. Geol.* **289**, 74–98 (2013).
104. L. Guangwei, L. Xiaohan, P. Alex, W. Lijie, L. Xiaobing, H. Feixin, Z. Xuejun, In-situ detrital zircon geochronology and Hf isotopic analyses from Upper Triassic Tethys sequence strata. *Earth Planet. Sci. Lett.* **297**, 461–470 (2010).
105. J.-G. Wang, F.-Y. Wu, X.-C. Tan, C.-Z. Liu, Magmatic evolution of the Western Myanmar Arc documented by U–Pb and Hf isotopes in detrital zircon. *Tectonophysics* **612–613**, 97–105 (2014).
106. F. Arboit, A. S. Collins, C. K. Morley, R. King, K. Amrouch, Detrital zircon analysis of the southwest Indochina terrane, central Thailand: Unravelling the Indosinian orogeny. *Geol. Soc. Am. Bull.* **128**, 1024–1043 (2016).
107. P. Castillo, C. M. Fanning, F. Hervé, J. P. Lacassie, Characterisation and tracing of Permian magmatism in the south-western segment of the Gondwanan margin; U–Pb age, Lu–Hf and O isotopic compositions of detrital zircons from metasedimentary complexes of northern Antarctic Peninsula and western Patagonia. *Gondwana Res.* **36**, 1–13 (2016).
108. B. Clements, I. Sevastjanova, R. Hall, E. A. Belousova, W. L. Griffin, N. Pearson, Detrital zircon U-Pb age and Hf-isotope perspective on sediment provenance and tectonic models in SE Asia. *Geol. Soc. Am. Spec. Pap.* **487**, 37–61 (2012).
109. J. Deng, X. Yang, Z.-F. Zhang, M. Santosh, Early Cretaceous arc volcanic suite in Cebu Island, Central Philippines and its implications on paleo-Pacific plate subduction: Constraints from geochemistry, zircon U–Pb geochronology and Lu–Hf isotopes. *Lithos* **230**, 166–179 (2015).
110. M. He, H. Zheng, P. D. Clift, Zircon U–Pb geochronology and Hf isotope data from the Yangtze River sands: Implications for major magmatic events and crustal evolution in Central China. *Chem. Geol.* **360–361**, 186–203 (2013).
111. K. D. Surpless, Z. T. Sickmann, T. A. Koplitz, East-derived strata in the Methow basin record rapid mid-Cretaceous uplift of the southern Coast Mountains batholith. *Can. J. Earth Sci.* **51**, 339–357 (2014).
112. S. Li, S. A. Wilde, Z. He, X. Jiang, R. Liu, L. Zhao, Triassic sedimentation and postaccretionary crustal evolution along the Solonker suture zone in Inner Mongolia, China. *Tectonics* **33**, 960–981 (2014).
113. H.-Y. Li, X.-L. Huang, Constraints on the paleogeographic evolution of the North China Craton during the Late Triassic–Jurassic. *J. Asian Earth Sci.* **70–71**, 308–320 (2013).
114. M.-D. Sun, Y.-G. Xu, S. A. Wilde, H.-L. Chen, Provenance of Cretaceous trench slope sediments from the Mesozoic Wandashan Orogen, NE China: Implications for determining ancient drainage systems and tectonics of the Paleo-Pacific. *Tectonics* **34**, 1269–1289 (2015).
115. J. Xu, Z. Li, Y. Shi, Jurassic detrital zircon U–Pb and Hf isotopic geochronology of Luxi Uplift, eastern North China, and its provenance implications for tectonic–paleogeographic reconstruction. *J. Asian Earth Sci.* **78**, 184–197 (2013).
116. C. Bao, Y.-L. Chen, D.-P. Li, X. Chen, Evolutionary history of Precambrian continental crust in the North China Craton. *Geochem. J.* **49**, 53–62 (2015).
117. A. Beltrán-Triviño, W. Winkler, A. Von Quadt, Tracing Alpine sediment sources through laser ablation U–Pb dating and Hf-isotopes of detrital zircons. *Sedimentology* **60**, 197–224 (2013).
118. J. J. Veevers, E. A. Belousova, A. Saeed, Zircons traced from the 700–500 Ma Transgondwanan Supermountains and the Gamburtsev Subglacial Mountains to the Ordovician Lachlan Orogen, Cretaceous Ceduna Delta, and modern Channel Country, central-southern Australia. *Sediment. Geol.* **334**, 115–141 (2016).
119. J. J. Veevers, A. Saeed, Age and composition of Antarctic sub-glacial bedrock reflected by detrital zircons, erratics, and recycled microfossils in the Ellsworth Land–Antarctic Peninsula–Weddell Sea–Dronning Maud Land sector (240°E–0°–015°E). *Gondwana Res.* **23**, 296–332 (2013).
120. J. J. Veevers, A. Saeed, Age and composition of Antarctic bedrock reflected by detrital zircons, erratics, and recycled microfossils in the Prydz Bay–Wilkes Land–Ross Sea–Marie Byrd Land sector (70°–240°E). *Gondwana Res.* **20**, 710–738 (2011).
121. R. Vadlamani, F.-Y. Wu, W.-Q. Ji, Detrital zircon U–Pb age and Hf isotopic composition from foreland sediments of the Assam Basin, NE India: Constraints on sediment provenance and tectonics of the Eastern Himalaya. *J. Asian Earth Sci.* **111**, 254–267 (2015).
122. Z. Zhang, W. Xiao, M. R. Majidifard, R. Zhu, B. Wan, S. Ao, L. Chen, M. Rezaeian, R. Esmaeili, Detrital zircon provenance analysis in the Zagros Orogen, SW Iran: Implications for the amalgamation history of the Neo-Tethys. *Int. J. Earth Sci.* (2016).
123. J. Slama, O. Walderhaug, H. Fonneland, J. Kosler, R. B. Pedersen, Provenance of Neoproterozoic to upper Cretaceous sedimentary rocks, eastern Greenland: Implications for recognizing the sources of sediments in the Norwegian Sea. *Sediment. Geol.* **238**, 254–267 (2011).
124. J.-G. Wang, F.-Y. Wu, E. Garzanti, X. Hu, W.-Q. Ji, Z.-C. Liu, X.-C. Liu, Upper Triassic turbidites of the northern Tethyan Himalaya (Langjiexue Group): The terminal of a sediment-routing system sourced in the Gondwanide Orogen. *Gondwana Res.* **34**, 84–98 (2016).
125. A. Mohammadi, J.-P. Burg, W. Winkler, J. Ruh, A. von Quadt, Detrital zircon and provenance analysis of Late Cretaceous–Miocene onshore Iranian Makran strata: Implications for the tectonic setting. *Geol. Soc. Am. Bull.* **128**, 1481 (2016).
126. A. I. S. Kemp, C. J. Hawkesworth, W. J. Collins, C. M. Gray, P. L. Blevin, Isotopic evidence for rapid continental growth in an extensional accretionary orogen: The Tasmanides, eastern Australia. *Earth Planet. Sci. Lett.* **284**, 455–466 (2009).
127. R. T. Tucker, E. M. Roberts, R. A. Henderson, A. I. S. Kemp, Large igneous province or long-lived magmatic arc along the eastern margin of Australia during the Cretaceous? Insights from the sedimentary record. *Geol. Soc. Am. Bull.* **128**, 1461–1480 (2016).
128. R. A. J. Robinson, C. A. Brezina, R. R. Parrish, M. S. A. Horstwood, N. W. Oo, M. I. Bird, M. Thein, A. S. Walters, G. J. H. Oliver, K. Zaw, Large rivers and orogens: The evolution of the Yarlung Tsangpo–Irrawaddy system and the eastern Himalayan syntaxis. *Gondwana Res.* **26**, 112–121 (2014).
129. J. Abati, A. M. Aghzer, A. Gerdes, N. Ennih, Insights on the crustal evolution of the West African Craton from Hf isotopes in detrital zircons from the Anti-Atlas belt. *Precambrian Res.* **212–213**, 263–274 (2012).
130. Y. Amelin, D.-C. Lee, A. N. Halliday, R. T. Pidgeon, Nature of the Earth's earliest crust from hafnium isotopes in single detrital zircons. *Nature* **399**, 252–255 (1999).

131. O. A. Anfinson, A. L. Leier, R. Gaschnig, A. F. Embry, K. Dewing, U–Pb and Hf isotopic data from Franklinian Basin strata: Insights into the nature of Crockerland and the timing of accretion, Canadian Arctic Islands. *Can. J. Earth Sci.* **49**, 1316–1328 (2012).
132. C. Augustsson, C. Munker, H. Bahlburg, C. M. Fanning, Provenance of late Palaeozoic metasediments of the SW South American Gondwana margin: A combined U–Pb and Hf-isotope study of single detrital zircons. *J. Geol. Soc.* **163**, 983–995 (2006).
133. D. Avigad, A. Gerdes, N. Morag, T. Bechstädt, Coupled U–Pb–Hf of detrital zircons of Cambrian sandstones from Morocco and Sardinia: Implications for provenance and Precambrian crustal evolution of North Africa. *Gondwana Res.* **21**, 690–703 (2012).
134. H. Bahlburg, J. D. Vervoort, S. A. Du Frane, B. Bock, C. Augustsson, C. Reimann, Timing of crust formation and recycling in accretionary orogens: Insights learned from the western margin of South America. *Earth Sci. Rev.* **97**, 215–241 (2009).
135. H. Bahlburg, J. D. Vervoort, S. A. DuFrane, Plate tectonic significance of Middle Cambrian and Ordovician siliciclastic rocks of the Bavarian Facies, Armorican Terrane Assemblage, Germany—U–Pb and Hf isotope evidence from detrital zircons. *Gondwana Res.* **17**, 223–235 (2010).
136. H. Bahlburg, J. D. Vervoort, S. Andrew DuFrane, V. Carlotto, C. Reimann, J. Cárdenas, The U–Pb and Hf isotope evidence of detrital zircons of the Ordovician Ollantaytambo Formation, southern Peru, and the Ordovician provenance and paleogeography of southern Peru and northern Bolivia. *J. South Am. Earth Sci.* **32**, 196–209 (2011).
137. L. P. Beranek, C. R. van Staal, W. C. McClelland, S. Israel, M. G. Mihalynuk, Detrital zircon Hf isotopic compositions indicate a northern Caledonian connection for the Alexander terrane. *Lithosphere* **5**, 163–168 (2013).
138. B. Bingen, W. L. Griffin, T. H. Torsvik, A. Saeed, Timing of Late Neoproterozoic glaciation on Baltica constrained by detrital zircon geochronology in the Hedmark Group, south-east Norway. *Terra Nova* **17**, 250–258 (2005).
139. J. Blichert-Toft, F. Albarède, Hafnium isotopes in Jack Hills zircons and the formation of the Hadean crust. *Earth Planet. Sci. Lett.* **265**, 686–702 (2008).
140. F. Choulet, D. Cluzel, M. Faure, W. Lin, B. Wang, Y. Chen, F.-Y. Wu, W. Ji, New constraints on the pre-Permian continental crust growth of Central Asia (West Junggar, China) by U–Pb and Hf isotopic data from detrital zircon. *Terra Nova* **24**, 189–198 (2012).
141. L. Duan, Q.-R. Meng, C.-L. Zhang, X.-M. Liu, Tracing the position of the South China block in Gondwana: U–Pb ages and Hf isotopes of Devonian detrital zircons. *Gondwana Res.* **19**, 141–149 (2011).
142. M. J. Flowerdew, I. L. Millar, M. L. Curtis, A. P. M. Vaughan, M. S. A. Horstwood, M. J. Whitehouse, C. M. Fanning, Combined U-Pb geochronology and Hf isotope geochemistry of detrital zircons from early Paleozoic sedimentary rocks, Ellsworth-Whitmore Mountains block, Antarctica. *Geol. Soc. Am. Bull.* **119**, 275–288 (2007).
143. Y. Geng, L. Du, L. Ren, Growth and reworking of the early Precambrian continental crust in the North China Craton: Constraints from zircon Hf isotopes. *Gondwana Res.* **21**, 517–529 (2012).
144. A. Gerdes, A. Zeh, Combined U–Pb and Hf isotope LA-(MC-)ICP-MS analyses of detrital zircons: Comparison with SHRIMP and new constraints for the provenance and age of an Armorican metasediment in Central Germany. *Earth Planet. Sci. Lett.* **249**, 47–61 (2006).
145. E. S. Grew, C. J. Carson, A. G. Christy, R. Maas, G. M. Yaxley, S. D. Boger, C. M. Fanning, New constraints from U–Pb, Lu–Hf and Sm–Nd isotopic data on the timing of sedimentation and felsic magmatism in the Larsemann Hills, Prydz Bay, East Antarctica. *Precambrian Res.* **206–207**, 87–108 (2012).
146. T. M. Harrison, J. Blichert-Toft, W. Müller, F. Albarede, P. Holden, S. J. Mojzsis, Heterogeneous Hadean hafnium: Evidence of continental crust at 4.4 to 4.5 Ga. *Science* **310**, 1947–1950 (2005).
147. T. M. Harrison, A. K. Schmitt, M. T. McCulloch, O. M. Lovera, Early (≥4.5 Ga) formation of terrestrial crust: Lu–Hf, $\delta^{18}O$, and Ti thermometry results for Hadean zircons. *Earth Planet. Sci. Lett.* **268**, 476–486 (2008).
148. N. Hauser, M. Matteini, R. H. Omarini, M. M. Pimentel, Combined U–Pb and Lu–Hf isotope data on turbidites of the Paleozoic basement of NW Argentina and petrology of associated igneous rocks: Implications for the tectonic evolution of western Gondwana between 560 and 460 Ma. *Gondwana Res.* **19**, 100–127 (2011).
149. B. Hu, M. Zhai, T. Li, Z. Li, P. Peng, J. Guo, T. M. Kusky, Mesoproterozoic magmatic events in the eastern North China Craton and their tectonic implications: Geochronological evidence from detrital zircons in the Shandong Peninsula and North Korea. *Gondwana Res.* **22**, 828–842 (2012).
150. P. Kaur, A. Zeh, N. Chaudhri, A. Gerdes, M. Okrusch, Archaean to Palaeoproterozoic crustal evolution of the Aravalli mountain range, NW India, and its hinterland: The U–Pb and Hf isotope record of detrital zircon. *Precambrian Res.* **187**, 155–164 (2011).
151. P. Kaur, A. Zeh, N. Chaudhri, A. Gerdes, M. Okrusch, Nature of magmatism and sedimentation at a Columbia active margin: Insights from combined U–Pb and Lu–Hf isotope data of detrital zircons from NW India. *Gondwana Res.* **23**, 1040–1052 (2013).
152. A. I. S. Kemp, C. J. Hawkesworth, B. A. Paterson, P. D. Kinny, Episodic growth of the Gondwana supercontinent from hafnium and oxygen isotopes in zircon. *Nature* **439**, 580–583 (2006).
153. N. B. Kuznetsov, L. M. Natapov, E. A. Belousova, S. Y. O'Reilly, W. L. Griffin, Geochronological, geochemical and isotopic study of detrital zircon suites from late Neoproterozoic clastic strata along the NE margin of the East European Craton: Implications for plate tectonic models. *Gondwana Res.* **17**, 583–601 (2010).
154. D. Li, Y. Chen, Z. Wang, K. Hou, C. Liu, Detrital zircon U–Pb ages, Hf isotopes and tectonic implications for Palaeozoic sedimentary rocks from the Xing-Meng orogenic belt, middle-east part of inner Mongolia, China. *Geol. J.* **46**, 63–81 (2011).
155. H.-Y. Li, B. He, Y.-G. Xu, X.-L. Huang, U–Pb and Hf isotope analyses of detrital zircons from Late Paleozoic sediments: Insights into interactions of the North China Craton with surrounding plates. *J. Asian Earth Sci.* **39**, 335–346 (2010).
156. L.-M. Li, M. Sun, Y. Wang, G. Xing, G. Zhao, Y. He, K. He, A. Zhang, U–Pb and Hf isotopic study of detrital zircons from the meta-sedimentary rocks in central Jiangxi Province, South China: Implications for the Neoproterozoic tectonic evolution of South China Block. *J. Asian Earth Sci.* **41**, 44–55 (2011).
157. X.-H. Li, Z.-X. Li, B. He, W.-X. Li, Q.-L. Li, Y. Gao, X.-C. Wang, The Early Permian active continental margin and crustal growth of the Cathaysia Block: In situ U–Pb, Lu–Hf and O isotope analyses of detrital zircons. *Chem. Geol.* **328**, 195–207 (2012).
158. C. Liu, G. Zhao, M. Sun, J. Zhang, Y. He, C. Yin, F. Wu, J. Yang, U-Pb and Hf isotopic study of detrital zircons from the Hutuo group in the Trans-North China Orogen and tectonic implications. *Gondwana Res.* **20**, 106–121 (2011).
159. C. Liu, G. Zhao, M. Sun, F. Wu, J. Yang, C. Yin, W. H. Leung, U–Pb and Hf isotopic study of detrital zircons from the Yejishan Group of the Lüliang Complex: Constraints on the timing of collision between the Eastern and Western Blocks, North China Craton. *Sediment. Geol.* **236**, 129–140 (2011).
160. C. Liu, G. Zhao, M. Sun, J. Zhang, C. Yin, Y. He, Detrital zircon U–Pb dating, Hf isotopes and whole-rock geochemistry from the Songshan Group in the Dengfeng Complex: Constraints on the tectonic evolution of the Trans-North China Orogen. *Precambrian Res.* **192–195**, 1–15 (2012).
161. C. Liu, G. Zhao, F. Liu, M. Sun, J. Zhang, C. Yin, Zircons U-Pb and Lu-Hf isotopic and whole-rock geochemical constraints on the Gantaohe Group in the Zanhuang Complex: Implications for the tectonic evolution of the Trans-North China Orogen. *Lithos* **146–147**, 80–92 (2012).
162. X. Liu, S. Gao, C. Diwu, W. Ling, Precambrian crustal growth of Yangtze Craton as revealed by detrital zircon studies. *Am. J. Sci.* **308**, 421–468 (2008).
163. X. Long, C. Yuan, M. Sun, W. Xiao, G. Zhao, Y. Wang, K. Cai, X. Xia, L. Xie, Detrital zircon ages and Hf isotopes of the early Paleozoic flysch sequence in the Chinese Altai, NW China: New constrains on depositional age, provenance and tectonic evolution. *Tectonophysics* **480**, 213–231 (2010).
164. Y. Luo, M. Sun, G. Zhao, S. Li, J. C. Ayers, X. Xia, J. Zhang, A comparison of U–Pb and Hf isotopic compositions of detrital zircons from the North and South Liaohe Groups: Constraints on the evolution of the Jiao-Liao-Ji Belt, North China Craton. *Precambrian Res.* **163**, 279–306 (2008).
165. X. Ma, L. Shu, B.-M. Jahn, W. Zhu, M. Faure, Precambrian tectonic evolution of Central Tianshan, NW China: Constraints from U–Pb dating and in situ Hf isotopic analysis of detrital zircons. *Precambrian Res.* **222–223**, 450–473 (2012).
166. N. Morag, D. Avigad, A. Gerdes, E. Belousova, Y. Harlavan, Crustal evolution and recycling in the northern Arabian-Nubian Shield: New perspectives from zircon Lu–Hf and U–Pb systematics. *Precambrian Res.* **186**, 101–116 (2011).
167. M. Petersson, thesis, Lund University, Lund, Sweden (2010).
168. A. B. Pietranik, C. J. Hawkesworth, C. D. Storey, A. I. S. Kemp, K. N. Sircombe, M. J. Whitehouse, W. Bleeker, Episodic, mafic crust formation from 4.5 to 2.8 Ga: New evidence from detrital zircons, Slave craton, Canada. *Geology* **36**, 875–878 (2008).
169. C. J. Spencer, C. W. Hoiland, R. A. Harris, P. K. Link, E. A. Balgord, Constraining the timing and provenance of the Neoproterozoic Little Willow and Big Cottonwood Formations, Utah: Expanding the sedimentary record for early rifting of Rodinia. *Precambrian Res.* **204–205**, 57–65 (2012).
170. C. J. Spencer, R. A. Harris, M. J. Dorais, Depositional provenance of the Himalayan metamorphic core of Garhwal region, India: Constrained by U–Pb and Hf isotopes in zircons. *Gondwana Res.* **22**, 26–35 (2012).
171. W.-H. Sun, M.-F. Zhou, J.-F. Gao, Y.-H. Yang, X.-F. Zhao, J.-H. Zhao, Detrital zircon U–Pb geochronological and Lu–Hf isotopic constraints on the Precambrian magmatic and crustal evolution of the western Yangtze Block, SW China. *Precambrian Res.* **172**, 99–126 (2009).
172. R. J. S. Teixeira, A. M. R. Neiva, P. B. Silva, M. E. P. Gomes, T. Andersen, J. M. F. Ramos, Combined U–Pb geochronology and Lu–Hf isotope systematics by LAM–ICPMS of zircons from granites and metasedimentary rocks of Carrazeda de Ansiães and Sabugal areas, Portugal, to constrain granite sources. *Lithos* **125**, 321–334 (2011).
173. O. M. Turkina, N. G. Berezhnaya, E. N. Lepekhina, I. N. Kapitonov, U–Pb (SHRIMP II), Lu–Hf isotope and trace element geochemistry of zircons from high-grade metamorphic rocks of the Irkut terrane, Sharyzhalgay Uplift: Implications for the Neoarchaean evolution of the Siberian Craton. *Gondwana Res.* **21**, 801–817 (2012).

174. Y. Wan, D. Liu, W. Wang, T. Song, A. Kröner, C. Dong, H. Zhou, X. Yin, Provenance of Meso- to Neoproterozoic cover sediments at the Ming Tombs, Beijing, North China Craton: An integrated study of U–Pb dating and Hf isotopic measurement of detrital zircons and whole-rock geochemistry. *Gondwana Res.* **20**, 219–242 (2011).
175. L. Wang, J. Yu, S. Y. O'Reilly, W. L. Griffin, T. Sun, Z. Wei, S. Jiang, L. Shu, Grenvillian orogeny in the Southern Cathaysia Block: Constraints from U-Pb ages and Lu-Hf isotopes in zircon from metamorphic basement. *Chin. Sci. Bull.* **53**, 3037–3050 (2008).
176. L.-J. Wang, W. L. Griffin, J.-H. Yu, S. Y. O'Reilly, Precambrian crustal evolution of the Yangtze Block tracked by detrital zircons from Neoproterozoic sedimentary rocks. *Precambrian Res.* **177**, 131–144 (2010).
177. W. Wang, M.-F. Zhou, D.-P. Yan, J.-W. Li, Depositional age, provenance, and tectonic setting of the Neoproterozoic Sibao Group, southeastern Yangtze Block, South China. *Precambrian Res.* **192–195**, 107–124 (2012).
178. Y. Wang, A. Zhang, W. Fan, G. Zhao, G. Zhang, Y. Zhang, F. Zhang, S. Li, Kwangsian crustal anatexis within the eastern South China Block: Geochemical, zircon U–Pb geochronological and Hf isotopic fingerprints from the gneissoid granites of Wugong and Wuyi–Yunkai Domains. *Lithos* **127**, 239–260 (2011).
179. L.-J. Wang, J.-H. Yu, W. L. Griffin, S. Y. O'Reilly, Early crustal evolution in the western Yangtze Block: Evidence from U–Pb and Lu–Hf isotopes on detrital zircons from sedimentary rocks. *Precambrian Res.* **222–223**, 368–385 (2012).
180. A. P. Willner, A. Gerdes, H.-J. Massonne, History of crustal growth and recycling at the Pacific convergent margin of South America at latitudes 29°–36° S revealed by a U–Pb and Lu–Hf isotope study of detrital zircon from late Paleozoic accretionary systems. *Chem. Geol.* **253**, 114–129 (2008).
181. X. Xia, M. Sun, G. Zhao, F. Wu, P. Xu, J. Zhang, Y. Luo, U–Pb and Hf isotopic study of detrital zircons from the Wulashan khondalites: Constraints on the evolution of the Ordos Terrane, Western Block of the North China Craton. *Earth Planet. Sci. Lett.* **241**, 581–593 (2006).
182. X. Xia, M. Sun, G. Zhao, F. Wu, P. Xu, J. Zhang, Y. He, Paleoproterozoic crustal growth in the Western Block of the North China Craton: Evidence from detrital zircon Hf and whole rock Sr-Nd isotopic compositions of the Khondalites from the Jining Complex. *Am. J. Sci.* **308**, 304–327 (2008).
183. J. Yao, L. Shu, M. Santosh, Detrital zircon U–Pb geochronology, Hf-isotopes and geochemistry—New clues for the Precambrian crustal evolution of Cathaysia Block, South China. *Gondwana Res.* **20**, 553–567 (2011).
184. J. Yao, L. Shu, M. Santosh, J. Li, Geochronology and Hf isotope of detrital zircons from Precambrian sequences in the eastern Jiangnan Orogen: Constraining the assembly of Yangtze and Cathaysia Blocks in South China. *J. Asian Earth Sci.* **74**, 225–243 (2013).
185. C. Yin, G. Zhao, J. Guo, M. Sun, X. Xia, X. Zhou, C. Liu, U–Pb and Hf isotopic study of zircons of the Helanshan Complex: Constrains on the evolution of the Khondalite Belt in the Western Block of the North China Craton. *Lithos* **122**, 25–38 (2011).
186. Q.-Z. Yin, J. Wimpenny, D. L. Tollstrup, M. Mange, J. F. Dewey, Q. Zhou, X.-H. Li, F.-Y. Wu, Q.-L. Li, Y. Liu, G.-Q. Tang, Crustal evolution of the South Mayo Trough, western Ireland, based on U–Pb ages and Hf–O isotopes in detrital zircons. *J. Geol. Soc.* **169**, 681–689 (2012).
187. J.-H. Yu, S. Y. O'Reilly, L. Wang, W. L. Griffin, M. Zhang, R. Wang, S. Jiang, L. Shu, Where was South China in the Rodinia supercontinent?: Evidence from U–Pb geochronology and Hf isotopes of detrital zircons. *Precambrian Res.* **164**, 1–15 (2008).
188. A. Zeh, A. Gerdes, Baltica- and Gondwana-derived sediments in the Mid-German Crystalline Rise (Central Europe): Implications for the closure of the Rheic ocean. *Gondwana Res.* **17**, 254–263 (2010).
189. A. Zeh, A. Gerdes, R. Klemd, J. M. Barton Jr., U–Pb and Lu–Hf isotope record of detrital zircon grains from the Limpopo Belt—Evidence for crustal recycling at the Hadean to early-Archean transition. *Geochim. Cosmochim. Acta* **72**, 5304–5329 (2008).
190. A. Zeh, A. Gerdes, C. Heubeck, U–Pb and Hf isotope data of detrital zircons from the Barberton Greenstone Belt: Constraints on provenance and Archaean crustal evolution. *J. Geol. Soc.* **170**, 215–223 (2013).
191. S.-B. Zhang, Y.-F. Zheng, Y.-B. Wu, Z.-F. Zhao, S. Gao, F.-Y. Wu, Zircon U–Pb age and Hf isotope evidence for 3.8 Ga crustal remnant and episodic reworking of Archean crust in South China. *Earth Planet. Sci. Lett.* **252**, 56–71 (2006).
192. J.-B. Zhou, S. A. Wilde, F.-L. Liu, J. Han, Zircon U–Pb and Lu–Hf isotope study of the Neoproterozoic Haizhou Group in the Sulu orogen: Provenance and tectonic implications. *Lithos* **136–139**, 261–281 (2012).
193. A. Zeh, A. Gerdes, U–Pb and Hf isotope record of detrital zircons from gold-bearing sediments of the Pietersburg Greenstone Belt (South Africa)—Is there a common provenance with the Witwatersrand Basin? *Precambrian Res.* **204–205**, 46–56 (2012).
194. N. Koglin, A. Zeh, H. E. Frimmel, A. Gerdes, New constraints on the auriferous Witwatersrand sediment provenance from combined detrital zircon U–Pb and Lu–Hf isotope data for the Eldorado Reef (Central Rand Group, South Africa). *Precambrian Res.* **183**, 817–824 (2010).
195. A. I. S. Kemp, S. A. Wilde, C. J. Hawkesworth, C. D. Coath, A. Nemchin, R. T. Pidgeon, J. D. Vervoort, S. A. DuFrane, Hadean crustal evolution revisited: New constraints from Pb–Hf isotope systematics of the Jack Hills zircons. *Earth Planet. Sci. Lett.* **296**, 45–56 (2010).
196. Y. Nebel-Jacobsen, C. Münker, O. Nebel, A. Gerdes, K. Mezger, D. R. Nelson, Reworking of Earth's first crust: Constraints from Hf isotopes in Archean zircons from Mt. Narryer, Australia. *Precambrian Res.* **182**, 175–186 (2010).
197. A. Zeh, R. A. Stern, A. Gerdes, The oldest zircons of Africa—Their U–Pb–Hf–O isotope and trace element systematics, and implications for Hadean to Archean crust–mantle evolution. *Precambrian Res.* **241**, 203–230 (2014).
198. A. Zeh, A. Gerdes, R. Klemd, J. M. Barton Jr., Archaean to Proterozoic crustal evolution in the central zone of the Limpopo Belt (South Africa–Botswana): Constraints from combined U–Pb and Lu–Hf isotope analyses of zircon. *J. Petrol.* **48**, 1605–1639 (2007).
199. A. Zeh, A. Gerdes, J. Barton Jr., R. Klemd, U–Th–Pb and Lu–Hf systematics of zircon from TTG's, leucosomes, meta-anorthosites and quartzites of the Limpopo Belt (South Africa): Constraints for the formation, recycling and metamorphism of Palaeoarchaean crust. *Precambrian Res.* **179**, 50–68 (2010).
200. D. W. Davis, Y. Amelin, G. M. Nowell, R. R. Parrish, Hf isotopes in zircon from the western Superior province, Canada: Implications for Archean crustal development and evolution of the depleted mantle reservoir. *Precambrian Res.* **140**, 132–156 (2005).
201. M. E. Bickford, P. A. Mueller, G. D. Kamenov, B. M. Hill, Crustal evolution of southern Laurentia during the Paleoproterozoic: Insights from zircon Hf isotopic studies of ca. 1.75 Ga rocks in central Colorado. *Geology* **36**, 555–558 (2008).
202. P. A. Mueller, G. D. Kamenov, A. L. Heatherington, J. Richards, Crustal Evolution in the Southern Appalachian Orogen: Evidence from Hf Isotopes in Detrital Zircons. *J. Geol.* **116**, 414–422 (2008).
203. D. Liu, S. A. Wilde, Y. Wan, S. Wang, J. W. Valley, N. Kita, C. Dong, H. Xie, C. Yang, Y. Zhang, L. Gao, Combined U–Pb, hafnium and oxygen isotope analysis of zircons from meta-igneous rocks in the southern North China Craton reveal multiple events in the Late Mesoarchean–Early Neoarchean. *Chem. Geol.* **261**, 140–154 (2009).
204. J. P. Zheng, W. L. Griffin, S. Y. O'Reilly, J. H. Zhao, Y. B. Wu, G. L. Liu, N. Pearson, M. Zhang, C. Q. Ma, Z. H. Zhang, C. M. Yu, Y. P. Su, H. Y. Tang, Neoarchean (2.7–2.8 Ga) accretion beneath the North China Craton: U–Pb age, trace elements and Hf isotopes of zircons in diamondiferous kimberlites. *Lithos* **112**, 188–202 (2009).
205. A. Gärtner, M. Villeneuve, U. Linnemann, A. Gerdes, N. Youbi, M. Hofmann, Similar crustal evolution in the western units of the Adrar Souttouf Massif (Moroccan Sahara) and the Avalonian terranes: Insights from Hf isotope data. *Tectonophysics* **681**, 305–317 (2016).
206. N. Chen, S. Gong, M. Sun, X. Li, X. Xia, Q. Wang, F. Wu, P. Xu, Precambrian evolution of the Quanji Block, northeastern margin of Tibet: Insights from zircon U–Pb and Lu–Hf isotope compositions. *J. Asian Earth Sci.* **35**, 367–376 (2009).
207. T. Iizuka, T. Komiya, S. P. Johnson, Y. Kon, S. Maruyama, T. Hirata, Reworking of Hadean crust in the Acasta gneisses, northwestern Canada: Evidence from in-situ Lu–Hf isotope analysis of zircon. *Chem. Geol.* **259**, 230–239 (2009).
208. C. J. Tochilin, G. E. Gehrels, J. Nelson, J. B. Mahoney, U-Pb and Hf isotope analysis of detrital zircons from the Banks Island assemblage (coastal British Columbia) and southern Alexander terrane (southeast Alaska). *Lithosphere* **6**, 200–215 (2014).
209. L. P. Beranek, C. R. van Staal, W. C. McClelland, S. Israel, M. G. Mihalynuk, Baltican crustal provenance for Cambrian–Ordovician sandstones of the Alexander terrane, North American Cordillera: Evidence from detrital zircon U–Pb geochronology and Hf isotope geochemistry. *J. Geol. Soc.* **170**, 7–18 (2013).
210. M. Kristoffersen, T. Andersen, A. Andresen, U–Pb age and Lu–Hf signatures of detrital zircon from Palaeozoic sandstones in the Oslo Rift, Norway. *Geol. Mag.* **151**, 816–829 (2014).
211. A. Andresen, N. Y. Agyei-Dwarko, M. Kristoffersen, N.-M. Hanken, A Timanian foreland basin setting for the late Neoproterozoic–Early Palaeozoic cover sequences (Dividal Group) of northeastern Baltica. *Geol. Soc. Spec. Publ.* **390**, 93–129 (2014).
212. N. B. Kuznetsov, E. A. Belousova, A. S. Alekseev, T. V. Romanyuk, New data on detrital zircons from the sandstones of the lower Cambrian Brusov Formation (White Sea region, East-European Craton): Unravelling the timing of the onset of the Arctida–Baltica collision. *Int. Geol. Rev.* **56**, 1945–1963 (2014).
213. C. J. Spencer, R. A. Harris, J. R. Major, Provenance of Permian–Triassic Gondwana Sequence units accreted to the Banda Arc in the Timor region: Constraints from zircon U–Pb and Hf isotopes. *Gondwana Res.* **38**, 28–39 (2016).
214. P. W. Haines, C. L. Kirkland, M. T. D. Wingate, H. Allen, E. A. Belousova, Y. Gréau, Tracking sediment dispersal during orogenesis: A zircon age and Hf isotope study from the western Amadeus Basin, Australia. *Gondwana Res.* **37**, 324–347 (2016).
215. X. Xia, X. Nie, C.-K. Lai, Y. Wang, X. Long, S. Meffre, Where was the Ailaoshan Ocean and when did it open: A perspective based on detrital zircon U–Pb age and Hf isotope evidence. *Gondwana Res.* **36**, 488–502 (2016).

216. B. J. Henderson, W. J. Collins, J. B. Murphy, G. Gutierrez-Alonso, M. Hand, Gondwanan basement terranes of the Variscan–Appalachian orogen: Baltican, Saharan and West African hafnium isotopic fingerprints in Avalonia, Iberia and the Armorican Terranes. *Tectonophysics* **681**, 278–304 (2016).
217. G. Meinhold, A. C. Morton, C. M. Fanning, J. P. Howard, R. J. Phillips, D. Strogen, A. G. Whitham, Insights into crust formation and recycling in North Africa from combined U–Pb, Lu–Hf and O isotope data of detrital zircons from Devonian sandstone of southern Libya. *Geol. Soc. Spec. Publ.* **386**, 281–292 (2013).
218. D. A. Foster, B. D. Goscombe, B. Newstead, B. Mapani, P. A. Mueller, L. C. Gregory, E. Muvangua, U–Pb age and Lu–Hf isotopic data of detrital zircons from the Neoproterozoic Damara Sequence: Implications for Congo and Kalahari before Gondwana. *Gondwana Res.* **28**, 179–190 (2015).
219. U. Linnemann, A. Gerdes, M. Hofmann, L. Marko, The Cadomian Orogen: Neoproterozoic to Early Cambrian crustal growth and orogenic zoning along the periphery of the West African Craton—Constraints from U–Pb zircon ages and Hf isotopes (Schwarzburg Antiform, Germany). *Precambrian Res.* **244**, 236–278 (2014).
220. C. R. Reimann, H. Bahlburg, E. Kooijman, J. Berndt, A. Gerdes, V. Carlotto, S. López, Geodynamic evolution of the early Paleozoic Western Gondwana margin 14°–17°S reflected by the detritus of the Devonian and Ordovician basins of southern Peru and northern Bolivia. *Gondwana Res.* **18**, 370–384 (2010).
221. B. McGee, A. S. Collins, R. I. F. Trindade, J. Payne, Age and provenance of the Cryogenian to Cambrian passive margin to foreland basin sequence of the northern Paraguay Belt, Brazil. *Geol. Soc. Am. Bull.* **127**, 76–86 (2015).
222. X.-Y. Zhu, F. Chen, S.-Q. Li, Y.-Z. Yang, H. Nie, W. Siebel, M.-G. Zhai, Crustal evolution of the North Qinling terrain of the Qinling Orogen, China: Evidence from detrital zircon U–Pb ages and Hf isotopic composition. *Gondwana Res.* **20**, 194–204 (2011).
223. Z.-W. Wang, F.-P. Pei, W.-L. Xu, H.-H. Cao, Z.-J. Wang, Y. Zhang, Tectonic evolution of the eastern Central Asian Orogenic Belt: Evidence from zircon U–Pb–Hf isotopes and geochemistry of early Paleozoic rocks in Yanbian region, NE China. *Gondwana Res.* **38**, 334–350 (2016).
224. J. Pertille, L. A. Hartmann, R. P. Philipp, T. S. Petry, C. de Carvalho Lana, Origin of the Ediacaran Porongos Group, Dom Feliciano Belt, southern Brazilian Shield, with emphasis on whole rock and detrital zircon geochemistry and U–Pb, Lu–Hf isotopes. *J. South Am. Earth Sci.* **64**, 69–93 (2015).
225. A. Abbo, D. Avigad, A. Gerdes, T. Güngör, Cadomian basement and Paleozoic to Triassic siliciclastics of the Taurides (Karacahisar dome, south-central Turkey): Paleogeographic constraints from U–Pb–Hf in zircons. *Lithos* **227**, 122–139 (2015).
226. D. Avigad, T. Weissbrod, A. Gerdes, O. Zlatkin, T. R. Ireland, N. Morag, The detrital zircon U–Pb–Hf fingerprint of the northern Arabian–Nubian Shield as reflected by a Late Ediacaran arkosic wedge (Zenifim Formation; subsurface Israel). *Precambrian Res.* **266**, 1–11 (2015).
227. M. A. Malkowski, B. A. Hampton, Sedimentology, U-Pb detrital geochronology, and Hf isotopic analyses from Mississippian–Permian stratigraphy of the Mystic subterrane, Farewell terrane, Alaska. *Lithosphere* **6**, 383–398 (2014).
228. F. Hervé, M. Calderón, C. M. Fanning, R. J. Pankhurst, E. Godoy, Provenance variations in the Late Paleozoic accretionary complex of central Chile as indicated by detrital zircons. *Gondwana Res.* **23**, 1122–1135 (2013).
229. A. P. Willner, S. M. Barr, A. Gerdes, H.-J. Massonne, C. E. White, Origin and evolution of Avalonia: Evidence from U–Pb and Lu–Hf isotopes in zircon from the Mira terrane, Canada, and the Stavelot–Venn Massif, Belgium. *J. Geol. Soc.* **170**, 769–784 (2013).
230. P. R. Eizenhöfer, G. Zhao, M. Sun, J. Zhang, Y. Han, W. Hou, Geochronological and Hf isotopic variability of detrital zircons in Paleozoic strata across the accretionary collision zone between the North China craton and Mongolian arcs and tectonic implications. *Geol. Soc. Am. Bull.* **127**, 1422–1436 (2015).
231. Y. Xu, P. A. Cawood, Y. Du, Z. Zhong, N. C. Hughes, Terminal suturing of Gondwana along the southern margin of South China Craton: Evidence from detrital zircon U-Pb ages and Hf isotopes in Cambrian and Ordovician strata, Hainan Island. *Tectonics* **33**, 2490–2504 (2014).
232. P. Li, G. Rosenbaum, J.-H. Yang, D. Hoy, Australian-derived detrital zircons in the Permian-Triassic Gympie terrane (eastern Australia): Evidence for an autochthonous origin. *Tectonics* **34**, 858–874 (2015).
233. D. Letsch, W. Winkler, A. von Quadt, D. Gallhofer, The volcano-sedimentary evolution of a post-Variscan intramontane basin in the Swiss Alps (Glarus Verrucano) as revealed by zircon U–Pb age dating and Hf isotope geochemistry. *Int. J. Earth Sci.* **104**, 123–145 (2015).
234. G. Hagen-Peter, J. M. Cottle, A. J. Tulloch, S. C. Cox, Mixing between enriched lithospheric mantle and crustal components in a short-lived subduction-related magma system, Dry Valleys area, Antarctica: Insights from U-Pb geochronology, Hf isotopes, and whole-rock geochemistry. *Lithosphere* **9**, 174–188 (2015).
235. X. Zhang, G. Zhao, M. Sun, P. R. Eizenhöfer, Y. Han, W. Hou, D. Liu, B. Wang, Q. Liu, B. Xu, Tectonic evolution from subduction to arc-continent collision of the Junggar ocean: Constraints from U-Pb dating and Hf isotopes of detrital zircons from the North Tianshan belt, NW China. *Geol. Soc. Am. Bull.* **128**, 644–660 (2016).
236. Y. Han, G. Zhao, M. Sun, P. R. Eizenhöfer, W. Hou, X. Zhang, D. Liu, B. Wang, G. Zhang, Paleozoic accretionary orogenesis in the Paleo-Asian Ocean: Insights from detrital zircons from Silurian to Carboniferous strata at the northwestern margin of the Tarim Craton. *Tectonics* **34**, 334–351 (2015).
237. D. Burianek, V. Janousek, P. Hanzl, Y. Jiang, K. Schulmann, O. Lexa, B. Altanbaatar, Petrogenesis of the Late Carboniferous Sagsai Pluton in the SE Mongolian Altai. *J. Geosci.* **61**, 67–92 (2016).
238. K. Cai, M. Sun, M. M. Buslov, B.-m. Jahn, W. Xiao, X. Long, H. Chen, B. Wan, M. Chen, E. S. Rubanova, A. V. Kulikova, E. E. Voytishek, Crustal nature and origin of the Russian Altai: Implications for the continental evolution and growth of the Central Asian Orogenic Belt (CAOB). *Tectonophysics* **674**, 182–194 (2016).
239. W.-H. Yao, Z.-X. Li, W.-X. Li, L. Su, J.-H. Yang, Detrital provenance evolution of the Ediacaran–Silurian Nanhua foreland basin, South China. *Gondwana Res.* **28**, 1449–1465 (2015).
240. A. Sagawe, A. Gärtner, U. Linnemann, M. Hofmann, A. Gerdes, Exotic crustal components at the northern margin of the Bohemian Massif—Implications from U–Th–Pb and Hf isotopes of zircon from the Saxonian Granulite Massif. *Tectonophysics* **681**, 234–249 (2016).
241. X. Xu, S. Y. O'Reilly, W. L. Griffin, X. Wang, N. J. Pearson, Z. He, The crust of Cathaysia: Age, assembly and reworking of two terranes. *Precambrian Res.* **158**, 51–78 (2007).
242. P. J. Voice, M. Kowalewski, K. A. Eriksson, Quantifying the timing and rate of crustal evolution: Global compilation of radiometrically dated detrital zircon grains. *J. Geol.* **119**, 109–126 (2011).
243. J. D. Vervoort, A. I. S. Kemp, Clarifying the zircon Hf isotope record of crust–mantle evolution. *Chem. Geol.* **425**, 65–75 (2016).
244. J.-J. Zhu, R.-Z. Hu, X.-W. Bi, H. Zhong, H. Chen, Zircon U–Pb ages, Hf–O isotopes and whole-rock Sr–Nd–Pb isotopic geochemistry of granitoids in the Jinshajiang suture zone, SW China: Constraints on petrogenesis and tectonic evolution of the Paleo-Tethys Ocean. *Lithos* **126**, 248–264 (2011).
245. S. Liu, C. Feng, B.-m. Jahn, R. Hu, S. Gao, I. M. Coulson, G. Feng, S. Lai, C. Yang, Y. Yang, Zircon U–Pb age, geochemical, and Sr–Nd–Hf isotopic constraints on the origin of mafic dykes in the Shaanxi Province, North China Craton, China. *Lithos* **175–176**, 244–254 (2013).
246. S. M. McDowell, S. Overton, C. M. Fisher, W. O. Frazier, C. F. Miller, J. S. Miller, R. C. Economos, Hafnium, oxygen, neodymium, strontium, and lead isotopic constraints on magmatic evolution of the supereruptive southern Black Mountains volcanic center, Arizona, U.S.A.: A combined LASS zircon–whole-rock study. *Am. Mineral.* **101**, 311–327 (2016).
247. D. Li, D. He, C. Fan, Geochronology and Sr–Nd–Hf isotopic composition of the granites, enclaves, and dikes in the Karamay area, NW China: Insights into late Carboniferous crustal growth of West Junggar. *Geosci. Front.* **6**, 153–173 (2015).
248. Y. Be'eri-Shlevin, Y. Katzir, J. Blichert-Toft, I. C. Kleinhanns, M. J. Whitehouse, Nd–Sr–Hf–O isotope provinciality in the northernmost Arabian–Nubian Shield: Implications for crustal evolution. *Contrib. Mineral. Petrol.* **160**, 181–201 (2010).
249. X.-C. Chen, R.-Z. Hu, X.-W. Bi, H. Zhong, J.-B. Lan, C.-H. Zhao, J.-J. Zhu, Zircon U–Pb ages and Hf–O isotopes, and whole-rock Sr–Nd isotopes of the Bozhushan granite, Yunnan province, SW China: Constraints on petrogenesis and tectonic setting. *J. Asian Earth Sci.* **99**, 57–71 (2015).
250. D. Tang, K. Qin, C. Li, L. Qi, B. Su, W. Qu, Zircon dating, Hf–Sr–Nd–Os isotopes and PGE geochemistry of the Tianyu sulfide-bearing mafic–ultramafic intrusion in the Central Asian Orogenic Belt, NW China. *Lithos* **126**, 84–98 (2011).
251. J.-H. Yang, F.-Y. Wu, S.-L. Chung, S. A. Wilde, M.-F. Chu, A hybrid origin for the Qianshan A-type granite, northeast China: Geochemical and Sr–Nd–Hf isotopic evidence. *Lithos* **89**, 89–106 (2006).
252. M. Ryan, thesis, San Jose State University, San Jose, CA (2011).
253. N. Jiang, J. Guo, Hannuoba intermediate-mafic granulite xenoliths revisited: Assessment of a Mesozoic underplating model. *Earth Planet. Sci. Lett.* **293**, 277–288 (2010).
254. Q.-F. Ding, S.-Y. Jiang, F.-Y. Sun, Zircon U–Pb geochronology, geochemical and Sr–Nd–Hf isotopic compositions of the Triassic granite and diorite dikes from the Wulonggou mining area in the Eastern Kunlun Orogen, NW China: Petrogenesis and tectonic implications. *Lithos* **205**, 266–283 (2014).
255. Z. Li, J.-S. Qiu, X.-S. Xu, Geochronological, geochemical and Sr–Nd–Hf isotopic constraints on petrogenesis of Late Mesozoic gabbro–granite complexes on the southeast coast of Fujian, South China: Insights into a depleted mantle source region and crust–mantle interactions. *Geol. Mag.* **149**, 459–482 (2012).
256. B.-m. Jahn, M. Usuki, T. Usuki, S.-L. Chung, Generation of Cenozoic granitoids in Hokkaido (Japan): Constraints from zircon geochronology, Sr-Nd-Hf isotopic and geochemical analyses, and implications for crustal growth. *Am. J. Sci.* **314**, 704–750 (2014).
257. S.-Y. Yang, S.-Y. Jiang, Y.-H. Jiang, K.-D. Zhao, H.-H. Fan, Geochemical, zircon U–Pb dating and Sr–Nd–Hf isotopic constraints on the age and petrogenesis of an Early

Cretaceous volcanic-intrusive complex at Xiangshan, Southeast China. *Mineral. Petrol.* **101**, 21–48 (2011).
258. S. Liu, R. Hu, S. Gao, C. Feng, Z. Huang, S. Lai, H. Yuan, X. Liu, I. M. Coulson, G. Feng, T. Wang, Y. Qi, U–Pb zircon, geochemical and Sr–Nd–Hf isotopic constraints on the age and origin of Early Palaeozoic I-type granite from the Tengchong–Baoshan Block, Western Yunnan Province, SW China. *J. Asian Earth Sci.* **36**, 168–182 (2009).
259. Y.-J. Lu, R. Kerrich, T. C. Mccuaig, Z.-X. Li, C. J. R. Hart, P. A. Cawood, Z.-Q. Hou, L. Bagas, J. Cliff, E. A. Belousova, S.-H. Tang, Geochemical, Sr–Nd–Pb, and zircon Hf–O isotopic compositions of Eocene–Oligocene shoshonitic and potassic adakite-like felsic intrusions in western Yunnan, SW China: Petrogenesis and tectonic implications. *J. Petrol.* **54**, 1309–1348 (2013).
260. K.-D. Zhao, S.-Y. Jiang, S.-Y. Yang, B.-Z. Dai, J.-J. Lu, Mineral chemistry, trace elements and Sr–Nd–Hf isotope geochemistry and petrogenesis of Cailing and Furong granites and mafic enclaves from the Qitianling batholith in the Shi-Hang zone, South China. *Gondwana Res.* **22**, 310–324 (2012).
261. J.-H. Yang, F.-Y. Wu, S. A. Wilde, F. Chen, X.-M. Liu, L.-W. Xie, Petrogenesis of an alkali syenite–granite–rhyolite suite in the Yanshan fold and Thrust belt, eastern north China Craton: Geochronological, geochemical and Nd–Sr–Hf isotopic evidence for lithospheric thinning. *J. Petrol.* **49**, 315–351 (2008).
262. S. Liu, R. Hu, S. Gao, C. Feng, G. Feng, I. M. Coulson, C. Li, T. Wang, Y. Qi, Zircon U–Pb age and Sr–Nd–Hf isotope geochemistry of Permian granodiorite and associated gabbro in the Songliao Block, NE China and implications for growth of juvenile crust. *Lithos* **114**, 423–436 (2010).
263. B. Li, S.-Y. Jiang, Q. Zhang, H.-X. Zhao, K.-D. Zhao, Geochemistry, geochronology and Sr–Nd–Pb–Hf isotopic compositions of Middle to Late Jurassic syenite–granodiorites–dacite in South China: Petrogenesis and tectonic implications. *Gondwana Res.* **35**, 217–237 (2016).
264. G.-C. Wang, Y.-H. Jiang, Z. Liu, C.-Y. Ni, L. Qing, Q. Zhang, Elemental and Sr-Nd-Hf isotopic constraints on the origin of Late Jurassic adakitic granodiorite in central Fujian province, southeast China. *Mineral. Petrol.* **109**, 501–518 (2015).
265. R. Xia, C. Wang, M. Qing, W. Li, E. J. M. Carranza, X. Guo, L. Ge, G. Zeng, Zircon U–Pb dating, geochemistry and Sr–Nd–Pb–Hf–O isotopes for the Nan'getan granodiorites and mafic microgranular enclaves in the East Kunlun Orogen: Record of closure of the Paleo-Tethys. *Lithos* **234–235**, 47–60 (2015).
266. X. Li, X. Mo, X. Huang, G. Dong, X. Yu, M. Luo, Y. Liu, U–Pb zircon geochronology, geochemical and Sr–Nd–Hf isotopic compositions of the Early Indosinian Tongren Pluton in West Qinling: Petrogenesis and geodynamic implications. *J. Asian Earth Sci.* **97**, 38–50 (2015).
267. J. Li, F. Guo, C. Li, L. Zhao, M. Huang, Permian back-arc extension in central Inner Mongolia, NE China: Elemental and Sr–Nd–Pb–Hf–O isotopic constraints from the Linxi high-MgO diabase dikes. *Isl. Arc* **24**, 404–424 (2015).
268. B. Luo, H. Zhang, X. Lü, U–Pb zircon dating, geochemical and Sr–Nd–Hf isotopic compositions of Early Indosinian intrusive rocks in West Qinling, central China: Petrogenesis and tectonic implications. *Contrib. Mineral. Petrol.* **164**, 551–569 (2012).
269. Y. Rojas-Agramonte, A. Kröner, A. García-Casco, T. Kemp, E. Hegner, M. Pérez, M. Barth, D. Liu, A. Fonseca-Montero, Zircon ages, Sr-Nd-Hf isotopic compositions, and geochemistry of granitoids associated with the northern ophiolite mélange of Central Cuba: Tectonic implication for Late Cretaceous magmatism in the Northwestern Caribbean. *Am. J. Sci.* **310**, 1453–1479 (2010).
270. Y. Cheng, C. Spandler, J. Mao, B. G. Rusk, Granite, gabbro and mafic microgranular enclaves in the Gejiu area, Yunnan Province, China: A case of two-stage mixing of crust- and mantle-derived magmas. *Contrib. Mineral. Petrol.* **164**, 659–676 (2012).
271. F. Yang, F. Chai, Z. Zhang, X. Geng, Q. Li, Zircon U–Pb geochronology, geochemistry, and Sr–Nd–Hf isotopes of granitoids in the Yulekenhalasu copper ore district, northern Junggar, China: Petrogenesis and tectonic implications. *Lithos* **190–191**, 85–103 (2014).
272. L. Liu, J.-S. Qiu, J.-L. Zhao, Z.-L. Yang, Geochronological, geochemical, and Sr–Nd–Hf isotopic characteristics of Cretaceous monzonitic plutons in western Zhejiang Province, Southeast China: New insights into the petrogenesis of intermediate rocks. *Lithos* **196–197**, 242–260 (2014).
273. D. Li, D. He, Y. Yang, Y. Lian, Petrogenesis of mid-Carboniferous volcanics and granitic intrusions from western Junggar Basin boreholes: Geodynamic implications for the Central Asian Orogenic Belt in Northwest China. *Int. Geol. Rev.* **56**, 1668–1690 (2014).
274. S.-Y. Zou, Z.-L. Li, B. Song, R. E. Ernst, Y.-Q. Li, Z.-Y. Ren, S.-F. Yang, H.-L. Chen, Y.-G. Xu, X.-Y. Song, Zircon U–Pb dating, geochemistry and Sr–Nd–Pb–Hf isotopes of the Wajilitag alkali mafic dikes, and associated diorite and syenitic rocks: Implications for magmatic evolution of the Tarim large igneous province. *Lithos* **212–215**, 428–442 (2015).
275. I. Peytcheva, A. von Quadt, N. Georgiev, Z. Ivanov, C. A. Heinrich, M. Frank, Combining trace-element compositions, U–Pb geochronology and Hf isotopes in zircons to unravel complex calcalkaline magma chambers in the Upper Cretaceous Srednogorie zone (Bulgaria). *Lithos* **104**, 405–427 (2008).
276. Z.-M. Yang, Y.-J. Lu, Z.-Q. Hou, Z.-S. Chang, High-Mg diorite from Qulong in southern Tibet: Implications for the genesis of adakite-like intrusions and associated porphyry Cu deposits in collisional orogens. *J. Petrol.* **56**, 227–254 (2015).
277. X.-H. Li, Z.-X. Li, W.-X. Li, Y. Liu, C. Yuan, G. Wei, C. Qi, U–Pb zircon, geochemical and Sr–Nd–Hf isotopic constraints on age and origin of Jurassic I- and A-type granites from central Guangdong, SE China: A major igneous event in response to foundering of a subducted flat-slab? *Lithos* **96**, 186–204 (2007).
278. J.-Y. Chen, J.-H. Yang, J.-H. Zhang, J.-F. Sun, S. A. Wilde, Petrogenesis of the Cretaceous Zhangzhou batholith in southeastern China: Zircon U–Pb age and Sr–Nd–Hf–O isotopic evidence. *Lithos* **162–163**, 140–156 (2013).
279. T. Wu, L. Xiao, S. A. Wilde, C.-Q. Ma, Z.-L. Li, Y. Sun, Q.-Y. Zhan, Zircon U–Pb age and Sr–Nd–Hf isotope geochemistry of the Ganluogou dioritic complex in the northern Triassic Yidun arc belt, Eastern Tibetan Plateau: Implications for the closure of the Garzê-Litang Ocean. *Lithos* **248–251**, 94–108 (2016).
280. T. Hou, Z. Zhang, J. Encarnacion, H. Huang, M. Wang, Geochronology/geochemistry of the Washan dioritic porphyry associated with Kiruna-type iron ores, Middle-Lower Yangtze River Valley, eastern China: Implications for petrogenesis/mineralization. *Int. Geol. Rev.* **54**, 1332–1352 (2012).
281. C. Wang, J. Deng, Y. Lu, L. Bagas, A. I. S. Kemp, T. C. McCuaig, Age, nature, and origin of Ordovician Zhibenshan granite from the Baoshan terrane in the Sanjiang region and its significance for understanding Proto-Tethys evolution. *Int. Geol. Rev.* **57**, 1922–1939 (2015).
282. P. Bouilhol, O. Jagoutz, J. M. Hanchar, F. O. Dudas, Dating the India–Eurasia collision through arc magmatic records. *Earth Planet. Sci. Lett.* **366**, 163–175 (2013).
283. A. Mohammadi, J.-P. Burg, P. Bouilhol, J. Ruh, U–Pb geochronology and geochemistry of Zahedan and Shah Kuh plutons, southeast Iran: Implication for closure of the South Sistan suture zone. *Lithos* **248–251**, 293–308 (2016).
284. A. Dolgopolova, R. Seltmann, R. Armstrong, E. Belousova, R. J. Pankhurst, I. Kavalieris, Sr–Nd–Pb–Hf isotope systematics of the Hugo Dummett Cu–Au porphyry deposit (Oyu Tolgoi, Mongolia). *Lithos* **164–167**, 47–64 (2013).
285. F.-B. Pan, H.-F. Zhang, W.-C. Xu, L. Guo, B.-J. Luo, S. Wang, U–Pb zircon dating, geochemical and Sr–Nd–Hf isotopic compositions of Motuo quartz–monzonite: Implication for the genesis and diversity of the high Ba–Sr granitoids in orogenic belt. *Tectonophysics* **668–669**, 52–64 (2016).
286. K.-D. Zhao, S.-Y. Jiang, W.-F. Chen, P.-R. Chen, H.-F. Ling, Zircon U–Pb chronology and elemental and Sr–Nd–Hf isotope geochemistry of two Triassic A-type granites in South China: Implication for petrogenesis and Indosinian transtensional tectonism. *Lithos* **160–161**, 292–306 (2013).
287. K.-D. Zhao, S.-Y. Jiang, T. Sun, W.-F. Chen, H.-F. Ling, P.-R. Chen, Zircon U–Pb dating, trace element and Sr–Nd–Hf isotope geochemistry of Paleozoic granites in the Miao'ershan–Yuechengling batholith, South China: Implication for petrogenesis and tectonic–magmatic evolution. *J. Asian Earth Sci.* **74**, 244–264 (2013).
288. W. Liu, X.-J. Liu, L.-J. Liu, Underplating generated A- and I-type granitoids of the East Junggar from the lower and the upper oceanic crust with mixing of mafic magma: Insights from integrated zircon U–Pb ages, petrography, geochemistry and Nd–Sr–Hf isotopes. *Lithos* **179**, 293–319 (2013).
289. W. Dan, X.-H. Li, Q. Wang, X.-C. Wang, D. A. Wyman, Y. Liu, Phanerozoic amalgamation of the Alxa Block and North China Craton: Evidence from Paleozoic granitoids, U–Pb geochronology and Sr–Nd–Pb–Hf–O isotope geochemistry. *Gondwana Res.* **32**, 105–121 (2016).
290. W. Dan, Q. Wang, X.-C. Wang, Y. Liu, D. A. Wyman, Y.-S. Liu, Overlapping Sr–Nd–Hf–O isotopic compositions in Permian mafic enclaves and host granitoids in Alxa Block, NW China: Evidence for crust–mantle interaction and implications for the generation of silicic igneous provinces. *Lithos* **230**, 133–145 (2015).
291. R. Wang, J. P. Richards, Z.-q. Hou, F. An, R. A. Creaser, Zircon U–Pb age and Sr–Nd–Hf–O isotope geochemistry of the Paleocene–Eocene igneous rocks in western Gangdese: Evidence for the timing of Neo-Tethyan slab breakoff. *Lithos* **224–225**, 179–194 (2015).
292. L. Chen, K.-Z. Qin, G.-M. Li, J.-X. Li, B. Xiao, J.-X. Zhao, X. Fan, Zircon U–Pb ages, geochemistry, and Sr–Nd–Pb–Hf isotopes of the Nuri intrusive rocks in the Gangdese area, southern Tibet: Constraints on timing, petrogenesis, and tectonic transformation. *Lithos* **212–215**, 379–396 (2015).
293. G.-M. Li, J.-X. Li, J.-X. Zhao, K.-Z. Qin, M.-J. Cao, N. J. Evans, Petrogenesis and tectonic setting of Triassic granitoids in the Qiangtang terrane, central Tibet: Evidence from U–Pb ages, petrochemistry and Sr–Nd–Hf isotopes. *J. Asian Earth Sci.* **105**, 443–455 (2015).
294. X.-C. Chen, R.-z. Hu, X.-W. Bi, H. Zhong, J.-B. Lan, C.-H. Zhao, J.-J. Zhu, Petrogenesis of metaluminous A-type granitoids in the Tengchong–Lianghe tin belt of southwestern China: Evidences from zircon U–Pb ages and Hf–O isotopes, and whole-rock Sr–Nd isotopes. *Lithos* **212–215**, 93–110 (2015).
295. X.-W. Li, X.-X. Mo, X.-H. Yu, Y. Ding, X.-F. Huang, P. Wei, W.-Y. He, Geochronological, geochemical and Sr–Nd–Hf isotopic constraints on the origin of the Cretaceous intraplate volcanism in West Qinling, Central China: Implications for asthenosphere–lithosphere interaction. *Lithos* **177**, 381–401 (2013).

296. Q. Shu, Y. Lai, Y. Zhou, J. Xu, H. Wu, Zircon U–Pb geochronology and Sr–Nd–Pb–Hf isotopic constraints on the timing and origin of Mesozoic granitoids hosting the Mo deposits in northern Xilamulun district, NE China. *Lithos* **238**, 64–75 (2015).
297. L. Yang, F. Chen, B.-X. Liu, Z.-P. Hu, Y. Qi, J.-D. Wu, J.-F. He, W. Siebel, Geochemistry and Sr–Nd–Pb–Hf isotopic composition of the Donggou Mo-bearing granite porphyry, Qinling orogenic belt, central China. *Int. Geol. Rev.* **55**, 1261–1279 (2013).
298. L. Ma, S.-Y. Jiang, B.-Z. Dai, Y.-H. Jiang, M.-L. Hou, W. Pu, B. Xu, Multiple sources for the origin of Late Jurassic Linglong adakitic granite in the Shandong Peninsula, eastern China: Zircon U–Pb geochronological, geochemical and Sr–Nd–Hf isotopic evidence. *Lithos* **162–163**, 251–263 (2013).
299. L.-L. Hao, Q. Wang, D. A. Wyman, Q. Ou, W. Dan, Z.-Q. Jiang, F.-Y. Wu, J.-H. Yang, X.-P. Long, J. Li, Underplating of basaltic magmas and crustal growth in a continental arc: Evidence from Late Mesozoic intermediate–felsic intrusive rocks in southern Qiangtang, central Tibet. *Lithos* **245**, 223–242 (2016).
300. H. Geng, M. Sun, C. Yuan, W. Xiao, W. Xian, G. Zhao, L. Zhang, K. Wong, F. Wu, Geochemical, Sr–Nd and zircon U–Pb–Hf isotopic studies of Late Carboniferous magmatism in the West Junggar, Xinjiang: Implications for ridge subduction? *Chem. Geol.* **266**, 364–389 (2009).
301. Q.-g. Zhai, B.-m. Jahn, L. Su, J. Wang, X.-X. Mo, H.-y. Lee, K.-l. Wang, S. Tang, Triassic arc magmatism in the Qiangtang area, northern Tibet: Zircon U–Pb ages, geochemical and Sr–Nd–Hf isotopic characteristics, and tectonic implications. *J. Asian Earth Sci.* **63**, 162–178 (2013).
302. Q.-g. Zhai, B.-m. Jahn, L. Su, R. E. Ernst, K.-l. Wang, R.-y. Zhang, J. Wang, S. Tang, SHRIMP zircon U–Pb geochronology, geochemistry and Sr–Nd–Hf isotopic compositions of a mafic dyke swarm in the Qiangtang terrane, northern Tibet and geodynamic implications. *Lithos* **174**, 28–43 (2013).
303. T. Liu, Q.-g. Zhai, J. Wang, P.-s. Bao, Z. Qiangba, S.-h. Tang, Y. Tang, Tectonic significance of the Dongqiao ophiolite in the north-central Tibetan plateau: Evidence from zircon dating, petrological, geochemical and Sr–Nd–Hf isotopic characterization. *J. Asian Earth Sci.* **116**, 139–154 (2016).
304. C. E. Ganade de Araujo, U. G. Cordani, R. F. Weinberg, M. A. S. Basei, R. Armstrong, K. Sato, Tracing Neoproterozoic subduction in the Borborema Province (NE-Brazil): Clues from U-Pb geochronology and Sr-Nd-Hf-O isotopes on granitoids and migmatites. *Lithos* **202–203**, 167–189 (2014).
305. U. Söderlund, P. J. Patchett, J. D. Vervoort, C. E. Isachsen, The ^{176}Lu decay constant determined by Lu–Hf and U–Pb isotope systematics of Precambrian mafic intrusions. *Earth Planet. Sci. Lett.* **219**, 311–324 (2004).
306. J. Blichert-Toft, F. Albarède, The Lu-Hf isotope geochemistry of chondrites and the evolution of the mantle-crust system. *Earth Planet. Sci. Lett.* **148**, 243–258 (1997).
307. G. Faure, *Principles of Isotope Geology* (Smith & Wyllie Intermediate Geology Series, John Wiley & Sons, 1977), 476 pp.
308. S. B. Jacobsen, G. J. Wasserburg, Sm-Nd isotopic evolution of chondrites. *Earth Planet. Sci. Lett.* **50**, 139–155 (1980).
309. S. K. Thompson, in *Sampling* (John Wiley & Sons, 2012), pp. 67–89.
310. G. Shields, J. Veizer, Precambrian marine carbonate isotope database: Version 1.1. *Geochem. Geophys. Geosyst.* **3**, 1–12 (2002).
311. M. R. Palmer, J. M. Edmond, The strontium isotope budget of the modern ocean. *Earth Planet. Sci. Lett.* **92**, 11–26 (1989).
312. D. Vance, D. A. H. Teagle, G. L. Foster, Variable Quaternary chemical weathering fluxes and imbalances in marine geochemical budgets. *Nature* **458**, 493–496 (2009).
313. A. C. Davis, M. J. Bickle, D. A. H. Teagle, Imbalance in the oceanic strontium budget. *Earth Planet. Sci. Lett.* **211**, 173–187 (2003).
314. R. E. Ernst, K. L. Buchan, Large mafic magmatic events through time and links to mantle-plume heads. *Geol. Soc. Am. Spec. Pap.* **352**, 483–575 (2001).

Acknowledgments: We thank G. J. Bowen, C.-T. Lee, and R. Mills for helpful discussions. We thank B. Schoene, C. Spencer, and F. Macdonald for their constructive review comments. **Funding:** C.P.B. and X.-M.L. acknowledge funding from X.-M.L.'s University of North Carolina at Chapel Hill startup fund. **Author contributions:** C.P.B. designed the project and compiled the data sets. C.P.B., A.W., and X.Y. performed the statistical analysis and model development. All authors contributed to the interpretation of the results and writing of the manuscript. **Competing interests:** The authors declare that they have no competing interests. **Data and materials availability:** All data needed to evaluate the conclusions in the paper are present in the paper and/or the Supplementary Materials. Additional data related to this paper may be requested from the authors.

Submitted 9 September 2016
Accepted 2 February 2017
Published 8 March 2017
10.1126/sciadv.1602183

Citation: C. P. Bataille, A. Willis, X. Yang, X.-M. Liu, Continental igneous rock composition: A major control of past global chemical weathering. *Sci. Adv.* **3**, e1602183 (2017).